Flash Flood Indicator

Petr Sercl, Martin Pecha, Petr Novak, Hana Kyznarova, Ondrej Ledvinka, Vojtech Svoboda, Jan Danhelka

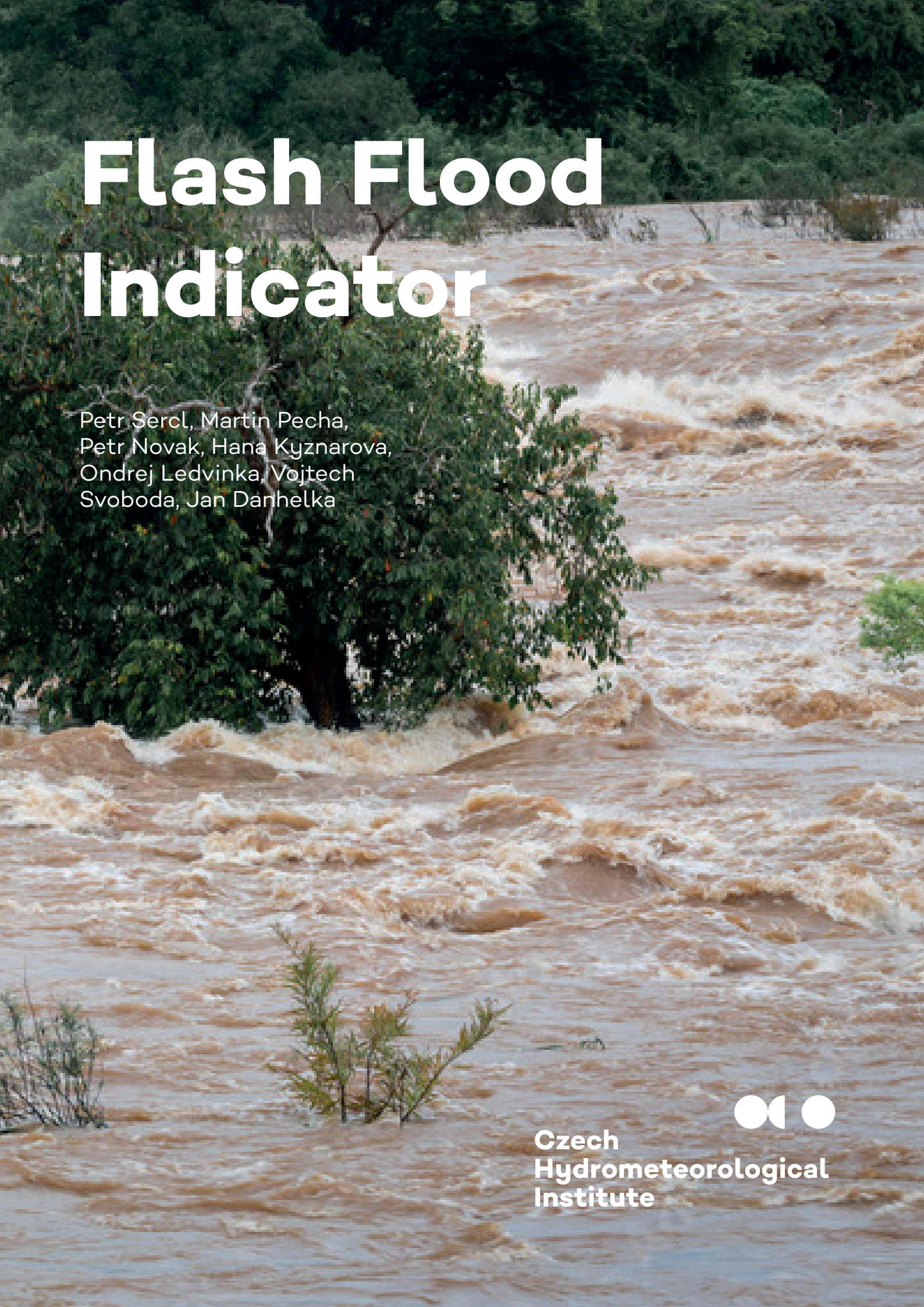

Czech Hydrometeorological Institute

Flash Flood Indicator

Petr Sercl, Martin Pecha, Petr Novak, Hana Kyznarova,
Ondrej Ledvinka, Vojtech Svoboda, Jan Danhelka

Prague 2023

Czech Hydrometeorological Institute

Collective of authors:

Petr Sercl, petr.sercl@chmi.cz

Martin Pecha, martin.pecha@chmi.cz

Petr Novak, petr.novak@chmi.cz

Hana Kyznarova, hana.kyznarova@chmi.cz

Ondrej Ledvinka, ondrej.ledvinka@chmi.cz

Vojtech Svoboda, vojtech.svoboda@chmi.cz

Jan Danhelka, jan.danhelka@chmi.cz

Czech Hydrometeorological Institute, Na Sabatce 2050/17, 143 06 Prague 12

Reviewer:

Milan Šálek

Jan Szturc

ISBN 978-80-7653-050-8

Contens

1. Introduction

This work deals with developing an operational approach to utilize the current possibilities of rainfall-runoff modelling for determining the risk of occurrence of flash floods in real-time. The report summarizes the results of research and development stemming from the sub-task "Development of a robust method for estimating runoff from heavy rainfall". This work was undertaken between 2008 and 2011 within the project SP/1c4/16/07 (Šercl et al. 2011).

This piece of research and development was inspired by the basic research reported in providing the Flash Flood Guidance (FFG), operated by the US National Weather Service (NWS) (Sweeney 1992). Its main output is the amount of rainfall of a given duration that is needed to cause bank-full conditions in smaller watercourses in the region, being dependent on the antecedent soil moisture conditions. This critical precipitation is termed the Flash Flood Guidance.

The research undertaken by the CHMI has resulted in development of a system that produces the Flash Flood Indicator that has been given the acronym FFI. The system was originally built using the ArcView GIS Avenue platform, with it being put into testing in June 2010 at the CHMI Hydrological Forecasting Department located in Prague. After three years of its operation, the system was transferred to ArcGIS using Python scripts.

The system contains three basic tools. These are:

a) Estimation of existing or "current" soil moisture conditions based on a daily time-step water balance of precipitation, runoff and actual evapotranspiration.

b) Derivation of the amount of precipitation of certain duration that may cause significant surface runoff in an area under the current soil moisture conditions.

c) Determination of the risk of occurrence of flash floods at specific locations based on up-to-date rainfall data and their short-term forecasts (nowcasting).

2. Definitions of Basic Terms

This chapter provides an explanation of several important terms used in this report. In particular, it is a matter of explaining the differences between 'local flooding' and 'flash flood' and explaining the term risk in the context of flash flood risk and local flooding risk.

Torrential rain

Torrential rain refers to the heavy downpour of rain. There is no unique definition of it other than the definition provided by the NWS. The NWS defines torrential rain as "rain that accumulates at a rate of three tenths of an inch or more per hour[1]" (Omondi 2017).

In terms of hydrology, the definition could be taken as the rainfall intensity that exceeds the rate at which soil can infiltrate and detain water, causing the affected area to generate surface runoff. The time of runoff concentration at the affected area may, depending on the intensity of rainfall and its duration, lead to so-called flash flooding.

Flash flood

Flash floods are caused by torrential rainfall usually caused by convective storm(s). It results in rapid runoff on slopes, in otherwise dry valleys and in watercourses. They are characterized by a rapid rise of the water level lasting in the order of minutes to units of hours and a significant impact of the dynamic force of turbulent flow as a factor in the occurrence of flood damage (Daňhelka et al. 2015).

A flash flood according to the American Meteorological Society is "Flooding with fast rise and fall times, which usually comes without warning and usually is the result of intense rain in a relatively small area". The NWS extends this definition to "... a rapid and extreme flow of high water into a normally dry area or a rapid rise in water flow above a predetermined level, indicating a flood hazard, with a rise time less than 6 hours ..." (NOAA 2010).

In the FFI concept, the term 'flash flood' is always meant to describe a hazardous event with attributes such as rapid rise of water level and high flow velocity. The risk of a flash flood occurrence (in short 'flash flood risk'; the term 'risk' is explained in more detail in the text below) is computed in hydraulically connected small river basins and river reaches, so the flash flood risk can be estimated not only for the catchments affected by torrential rain, but also for the catchments located downstream.

Local flooding

The term 'local flooding' describes situations where torrential rainfall is expected to cause high runoff volumes in small catchments or localized areas with minimal impact on main streams.

In the FFI concept, local flooding is always directly connected with a territory affected by torrential rain. It is assumed that pluvial flooding in urbanized areas is the main consequence of torrential rain. The risk of local flooding is estimated independently for individual grid cells, which are not hydraulically connected.

Risk

The term 'risk' is used throughout the report in the context of the risk of flash floods or local flooding occurrence. The risk can be expressed as a resulting value of the following formula:

Risk = hazard × (vulnerability × exposure)

The hazard is represented by potential or falling torrential rain over some specific place or territory, causing rapid runoff. In case of torrential rainfalls and flash floods, a threat to the life of people is understood to be the main aspect of vulnerability; however, economic damage is often associated with flash floods as well, especially in cases of high density of settlements in the affected area. The exposure includes not only the aspects such as urban areas and village settlements, which are of high density even in headwater areas in Czechia, but also transportation infrastructure and popular outdoor activities like canoeing, camping, and hiking. Based on the above-mentioned facts, it was concluded that no stream could be excluded from the definition of the exposed territory, as all streams might experience the presence of people who are the main factor of vulnerability. It is therefore assumed that the best real-time estimate of the imminent flash flood risk equals the estimate of relative flash flood magnitude in a given area as compared to the theoretical Q_{100} value.

The general risk is possible to express as a combination of flash flood risk and local flooding risk, where the risk of local flooding is considered potentially less dangerous.

1 7.6 mm per hour or more


AP10 AM 3199
AP 9 L 2324

3. Current Possibilities of Operative Forecasts of Torrential Rainfall and Flash Floods

Rainfall associated with cumulonimbus clouds (Cb) is one of the phenomena resulting in severe convective storms. In Czechia, the most common cause of torrential rainfall of long duration (ranging from tens of minutes to several hours) is the slow progress of supercells or multicell storms, respectively, termed mesoscale convective systems (Řezáčová et al. 2007). Another cause of long-lasting torrential rainfall is the so-called 'train' effect. This is a configuration of a series of storm cells that occur over time, with individual storm cells being formed at a particular place and then progressing along the same trajectory. That results in torrential rainfall of extreme amount affecting the same areas.

The formation of these types of convective storms is very dynamic, and it is therefore very complicated to predict the exact location of the torrential rainfall occurrence and, hence, the location of potential flash floods, even with the existing local area numerical weather prediction models, e.g., ALADIN.

While the regional flooding in both the summer and winter half of the year is predictable, and can also be well monitored thanks to the relatively dense network of water-gauging stations, flash floods are quite differing. The main reason for this is a relatively small area (mostly up to tens of km^2), which is affected by heavy rainfall intensities, and the onset of the resultant floods that usually occur very rapidly.

One of the ways of achieving a prompt forecast of a potential flash flood in an operational setting is by processing the data from weather radar and automatic rainfall stations in the shortest possible time step and an automatic recalculation (transposition) to the individual river basins of interest. At the same time, the so-called nowcasting tools must be available, i.e., tools to timely predict the possible progress of existing convective systems. The case study by Šálek et al. (2006) sets out the following criteria for developing an effective flood warning system:

a) provision of quantitative precipitation estimates based on reliable weather radar measurements,

b) availability of nowcasting prediction for each radar measurement interval,

c) hydrological rainfall-runoff modelling that allows processing of every radar interval measurement,

d) setting the size of the elementary catchment close to the horizontal dimensions of the convective storms,

e) continuous data flow into the system enabling timely alerting.

4. Description of Methodological Procedures

Figure 4.1 below shows a schematic diagram of the FFI functioning, distinguishing graphically the inputs, outputs and processes that take place in the system. Numbers in brackets represent references to individual sub-chapters.

4.1 Estimating the areal distribution of soil moisture

The amount of direct runoff resulting from rainfall is significantly influenced by the antecedent soil moisture conditions of the affected area, and more precisely, the actual retention deficit of the area. The retention capacity of the area is given by land cover (land use) and hydropedological (soil) characteristics.

The soil moisture retention capacity (A) of the area can be expressed by applying the CN parameter value using the relation:

$$A = 25.4 \cdot \left(\frac{1000}{CN} - 10\right) [\text{mm}]. \qquad (4.1)$$

The CN parameter is mainly used to determine the amount of direct runoff based on rainfall that has occurred. The CN principle is described in detail in the literature, e.g., Hawkins (1978).

The CN is expressed as a dimensionless value that depends on the infiltration capacity of the soil surface, the moisture retention capacity of the soil, and the land use pattern that directly affects the infiltration capacity.

In the sloping area, however, on top of the retention capacity of the soil, the gravitational force plays great role, with water flowing through the so-called preferential paths either on the surface (a network of permanent or ephemeral streams) or, in the case of permeable soils, as rapid sub-surface (hypodermic) runoff just below the surface. In reality, usually a combination of these phenomena occurs. Therefore, it can be assumed that the amount of direct runoff will be greater in areas having a slope than in those that are flat.

In order to improve determination of CN values, the soils were categorized into hydrological groups (primarily determined by soil permeability) along with their infiltration capacities, water retention capacity and the average slope of the area derived from a digital elevation model.

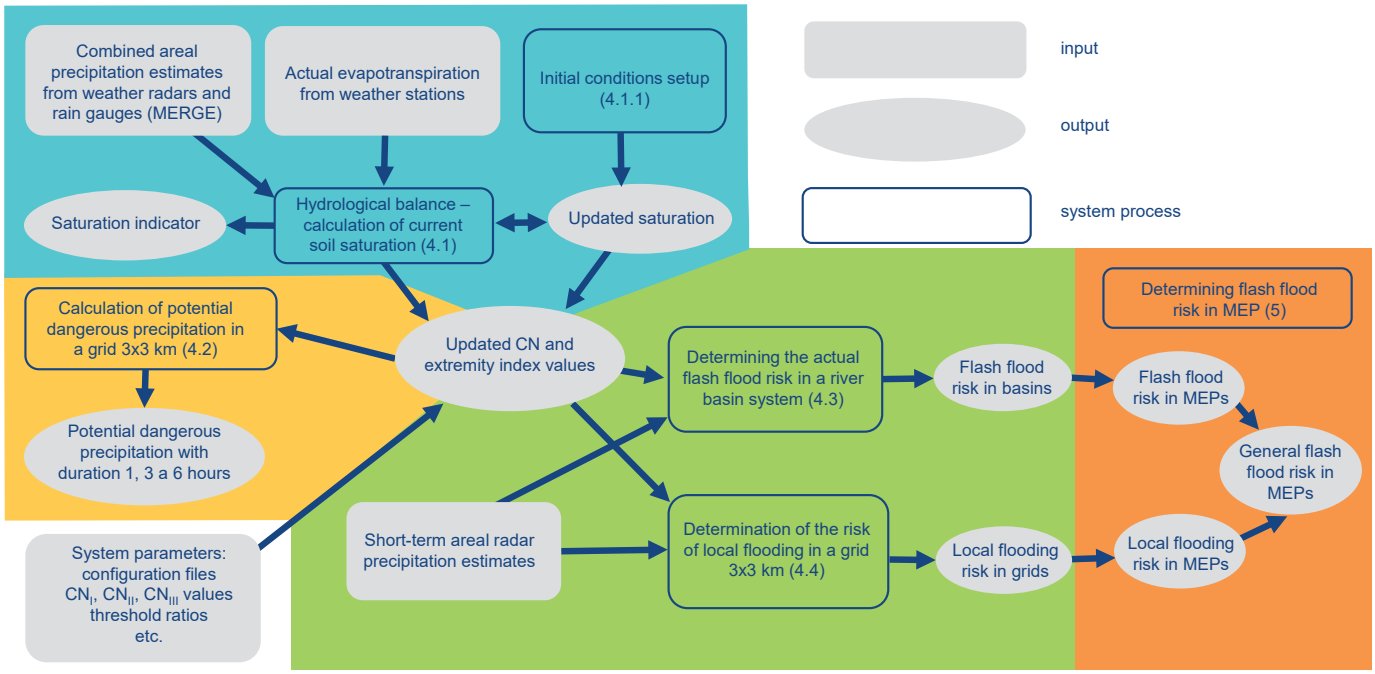

Fig. 4.1 Schematic diagram of the FFI functioning.

New *CN* values (see Fig. 4.2) were derived using the data on hydropedological characteristics, which were among the results of a research project (Říčicová et al. 2007) and were provided by the Research Institute for Soil and Water Conservation (RISWC).

The *CN* values have been prepared in accordance with the methodology described in the research project (Říčicová et al. 2007), and represent the "average" moisture conditions. The *CN* value corresponding to these conditions is generally referred to as the CN_{II}. It can be concluded that in the dry season, or vice versa, in the wet season, the *CN* value will change significantly, but will remain within certain limits. These limits and their respective values are referred to as CN_{I} (dry conditions) and CN_{III} (wet conditions).

The following formulas for calculating CN_{I} and CN_{III} have been taken from Kovář (1990):

$$CN_I = \frac{CN_{II}}{2.334 - 0.01334 \cdot CN_{II}}, \qquad (4.2)$$

$$CN_{III} = \frac{CN_{II}}{0.4036 + 0.005964 \cdot CN_{II}}. \qquad (4.3)$$

The corresponding soil moisture retention capacity values, indicated as A_{I} and A_{III}, are determined according to Equation (4.1).

The soil moisture retention potential is considered to be in the range from zero, when the soil is fully saturated and unable to absorb additional water, to the specified maximum value (difficult to accurately estimate), when the upper soil layers are dry. During this dry condition, plants cannot take up more water from the soil, and actual evapotranspiration is zero. In our case, the value of potential retention capacity (A_{I}) is estimated from the corresponding CN_{I} value using Equation (4.2).

The total potential retention R will then be the sum of the current potential soil retention (A) and the soil surface retention, which is commonly estimated as $0.2 \cdot A$, see Equation (4.6).

If we denote the size of the total potential retention at time t_1 as R_{t1} and, analogously, at time t_2 as R_{t2}, the mass balance equation can be written in the form:

$$R_{t2} = R_{t1} + ET - (H_s - H_o - H_{PZV}), \qquad (4.4)$$

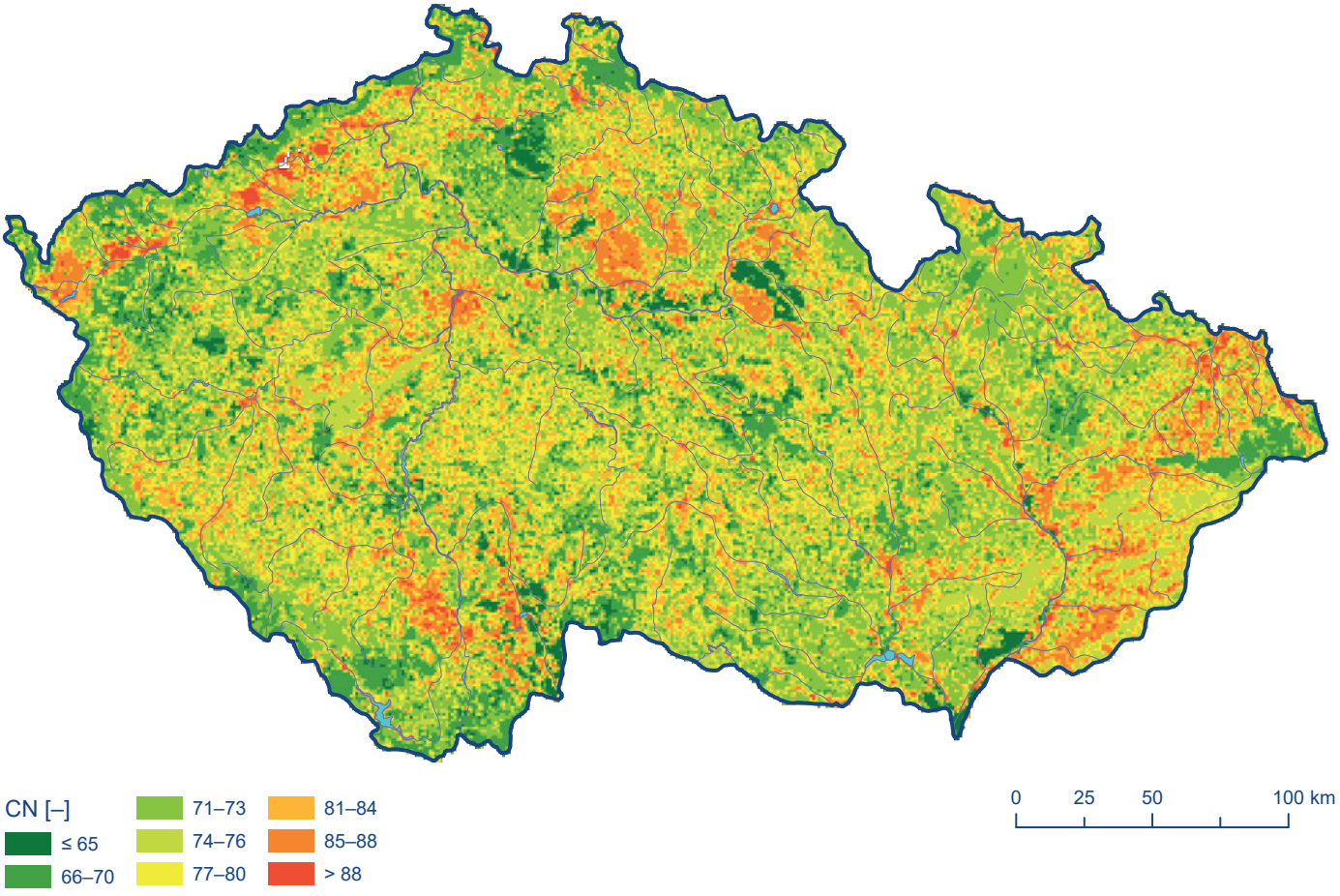

Fig. 4.2 CN_{II} values in a raster of 100×100 m.

where

ET is the value of actual evapotranspiration [mm] in time interval $t_2 - t_1$,

H_s is amount of rainfall [mm] that has occurred in time interval $t_2 - t_1$,

H_o is amount of direct (surface) runoff [mm] in time interval $t_2 - t_1$, determined from Equation (4.5),

H_{PZV} is water loss due to infiltration into deeper soil layers – percolation [mm] in time interval $t_2 - t_1$.

$$H_o = \frac{(H_S - 0.2 \cdot A)^2}{H_S + 0.8 \cdot A}, \text{ where } H_s \geq 0.2 \cdot A. \quad (4.5)$$

The interval of 24 hours is considered the time step for the calculation of $(t_2 - t_1)$. The calculation algorithm was prepared in the GIS environment, with all data inputs and outputs being in a raster representation.

The total potential retention can be obtained from the relation:

$$R = A + 0.2 \cdot A, \quad (4.6)$$

where

A is potential retention [mm] of the subsurface zone (soil), determined according to Equation (4.1),

$0.2 \cdot A$ is soil surface retention [mm], i.e., mainly interception and accumulation in small depressions.

The raster calculation of the actual evapotranspiration (ET) is based on the interpolation of point values by the Inverse Distance Weighting (IDW) method. The point values of ET are derived from the measurements of meteorological elements carried out by the CHMI using the modified Penmann-Monteith method. The method is described by Kohut et al. (2011).

The input raster of rainfall totals H_s, within the operational regime of the FFI system, represents the rainfall estimates as a combination of weather radar data and rain gauge observations (Novák, Kyznarová 2014).

In terms of the approach, the magnitude of percolation H_{PZV} is the most problematic element of Equation (4.4). Its value may be non-zero if there is some moisture surplus in the upper soil layers that cannot be removed by evapotranspiration. In the proposed algorithm, the value of H_{PZV} is estimated from the relationships:

$$H_{PZVi} = k_1 \cdot \left(H_{s(i-1)} - H_{o(i-1)} - ET_{i-1}\right) + k_2 \cdot H_{PZV(i-1)}, \text{ if } H_{s(i-1)} - H_{o(i-1)} > ET_{i-1}, \quad (4.7)$$

$$H_{PZVi} = k_2 \cdot H_{PZV(i-1)}, \text{ if } H_{s(i-1)} - H_{o(i-1)} \leq ET_{i-1}, \quad (4.8)$$

where

H_{PZVi} is percolation on the i-th day [mm],

$H_{PZV(i-1)}$ is percolation on day $(i - 1)$ [mm],

k_1, k_2 are coefficients.

The coefficient k_1 in Equation (4.7) is assumed to be 0.1 over the whole territory of Czechia. This means that after deduction of evapotranspiration and runoff, 90% of water remains in the soil, while 10% of water flows through percolation into deeper soil horizons.

The coefficient k_2 expresses the saturation of soil layers when the actual retention potential A_i is less than the retention under average moisture conditions A_{II} and the soil moisture above field capacity. The value of the coefficient k_2 is therefore zero if the actual retention A_i is higher than the value of A_{II} (soil moisture is lost only by evapotranspiration, and it is not lost to groundwater during the period of rainfall). It reaches its highest value when the actual retention is lower than the value of A_{III} (the soil is heavily saturated and drains to deeper soil layers). In a situation where the retention is lower than A_{II} but higher than A_{III}, the value of the coefficient k_2 for the i-th day is calculated from the formula:

$$k_{2i} = k_{2\max} \cdot \frac{A_{II} - A_{i-1}}{A_{II} - A_{III}}. \quad (4.9)$$

The value of k_{2max} is considered 0.9 and remains constant if actual potential retention is lower than A_{III}.

The current total retention potential R_i can be converted according to Equation (4.6) to the retention of subsurface layer A_i, and the actual value of CN_i can be derived by Equation (4.1).

The actual value of soil moisture may not be obvious from the actual retention potential A_i at first glance, since the retention potential limit values can vary among various soil types. Therefore, a certain coefficient (or indicator) has been defined to express the current level of soil moisture content relative to the limit values.

The saturation indicator is expressed as:

$$U_{Ni} = \frac{-A_i - A_{II}}{A_I - A_{II}}, \text{ if } A_i \geq A_{II}, \quad (4.10)$$

$$U_{Ni} = \frac{A_{II} - A_i}{A_{II} - A_{III}}, \text{ if } A_i < A_{II}. \quad (4.11)$$

The A_I, A_{II} and A_{III} values in Equations (4.10) and (4.11) correspond to the CN_I, CN_{II} and CN_{III} values respectively, see Equations (4.1), (4.2) and (4.3).

The defined saturation indicator U_N takes values from −1 to +1 in the case where the values of A_I and A_{III} are set as the limits that cannot be exceeded. However, experience has shown that only the A_I value can be considered as the limit value, while the value of A_{III} can be theoretically exceeded, since each soil layer can reach the state of full saturation (when A_i value equals zero over the short term). Therefore, the indicator U_N exceeds +1 when $A_i < A_{III}$.

The fact is that areas with relatively high A_{II} values (soils with high infiltration capacity) also have a corresponding higher dry state threshold, i.e., the retention potential A_I values.

The relationship between the CN value and the retention potential A [mm] is apparent from Fig. 4.3. It is clear that for lower CN values, the retention potential increases to very high, even unrealistic, figures.

For these reasons, a certain modification of Equation (4.10) has been proposed, where the U_N value obtained according to Equation (4.10) is multiplied by a correction coefficient, expressing the amount of water, in mm, which must evaporate or drain to increase the retention by 1%:

$$U_{Ni} = \frac{-A_i - A_{II}}{A_I - A_{II}} \cdot \frac{A_I - A_{II}}{100}, \text{ if } A_i \geq A_{II}. \quad (4.12)$$

Specific value intervals of the U_N indicator were characterized verbally, as indicated in Tab. 4.1.

The above-described methodology using a daily water balance to estimate soil moisture retention potential changes was tested in the project (Řičicová et al. 2007) at ten pilot river basins for 2002, 2003 and 2006 conditions, where it proved its functionality in the basins located in the crystalline complex and in the flysch areas. The calculation failed only in basins representing the extremely permeable area of the Bohemian Cretaceous Basin, because the hydrological regime there is very specific, with extremely low variability of discharge and presence of threshold processes in complex geological structures. The criterion used to verify credibility of the method involved the statistically significant agreement (in terms of the coefficient of determination) in the temporal variation of the saturation indicator versus the corresponding mean daily river flows.

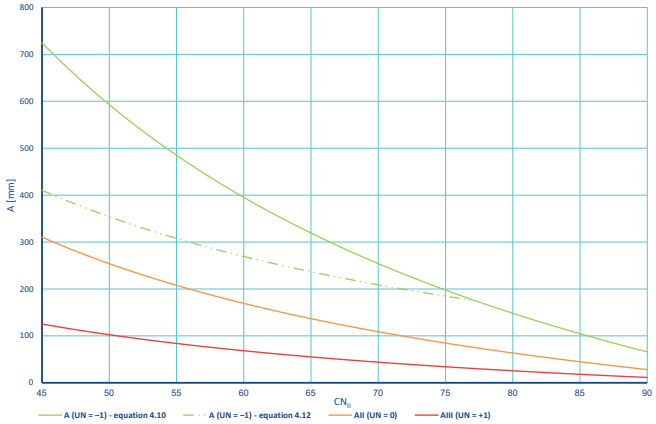

Fig. 4.3 Relation of the retention potential *A* [mm] to the *CN* value for saturation indicators equal to −1, 0 and +1. The dashed line shows a modification of the saturation indicator calculated according to Equation (4.12).

Tab. 4.1 Verbal expression of the state of soil moisture of the area according to the range of values of the U_N soil saturation indicator.

U_N value range	Description
≤ −0.7	Very low saturation
−0.69 to −0.3	Low saturation
−0.29 to +0.3	Saturation at field capacity
+0.31 to +0.7	High saturation
+0.71 to +1	Very high saturation
> +1	Extremely high saturation

Figure 4.4 provides an example of a map output with the spatial distribution of the values of the soil saturation indicator valid for July 19, 2020 at 06:00 UTC.

4.1.1 Determination of initial conditions for modelling

The model real-time simulation must start under certain predetermined initial conditions. The modelling starts at the beginning of the spring period (early April), when evapotranspiration is still quite negligible and the soil is soaked with water from previous precipitation or snowmelt. The values of current soil moisture conditions should be set so that they reflect the previous weather characteristics (rain-

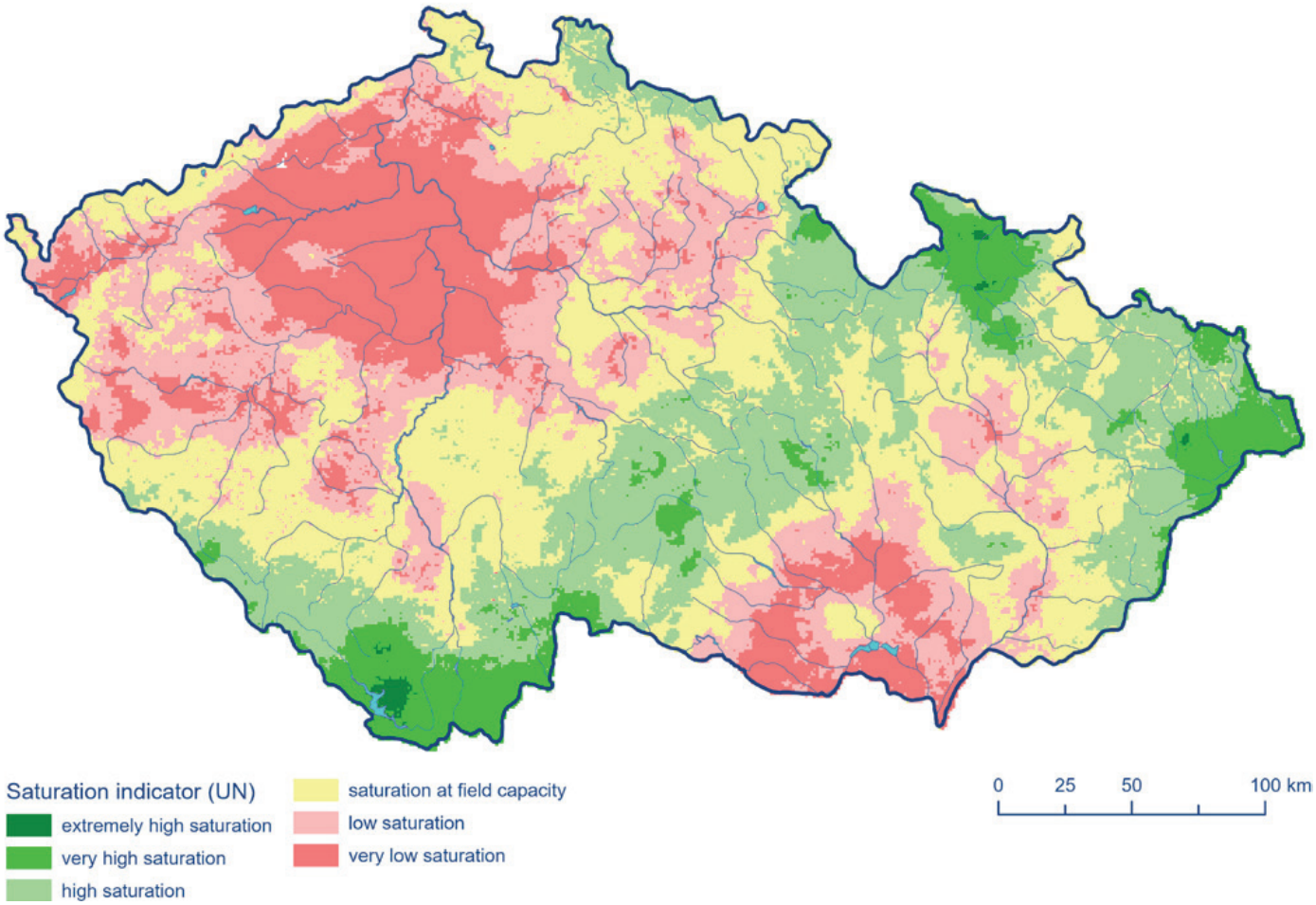

Fig. 4.4 Example of soil saturation indicator (U_N) values valid for July 19, 2020 at 06:00 UTC.

fall, air temperature, snow melting). This task is relatively difficult and subjective, see Chapter 6.2.

4.2 Derivation of potential dangerous rainfall

4.2.1 The flash flood risk and the Extremity Index

As already mentioned above, it is very difficult to predict the occurrence of a flash flood (i.e., flash flood risk) for a specific territory and to warn the population in time, especially as numerical weather prediction models cannot determine the timing and the river catchment(s) hit by the anticipated torrential rainfall with sufficient accuracy and lead time.

However, based on the information on the antecedent soil moisture conditions and physical-geographical characteristics of the area, it is possible:

- to estimate the magnitude of potential dangerous rainfall of a given duration that, if occurs, may cause surface runoff of a specified significance in the area; and
- to determine the imminent risk of a flash flood in a specific area based on current rainfall data (e.g., from weather radar measurements) and very short-term forecasts of significant rainfall using nowcasting.

In order to determine the above values, it is helpful to have a reference value to determine or estimate the magnitude of potential flash flood risk. For this purpose, the theoretical value of the 100-year specific runoff q_{100} was chosen, where specific runoff is simply Q/CA (Q is discharge and CA means catchment area).

However, for small size river basins or small areas for which the calculation of potential dangerous rainfall or the imminent flash flood risk is needed, direct hydrological observations are usually not available, so q_{100} must be estimated using indirect methods, if available, such as regional formulas or regression relationships.

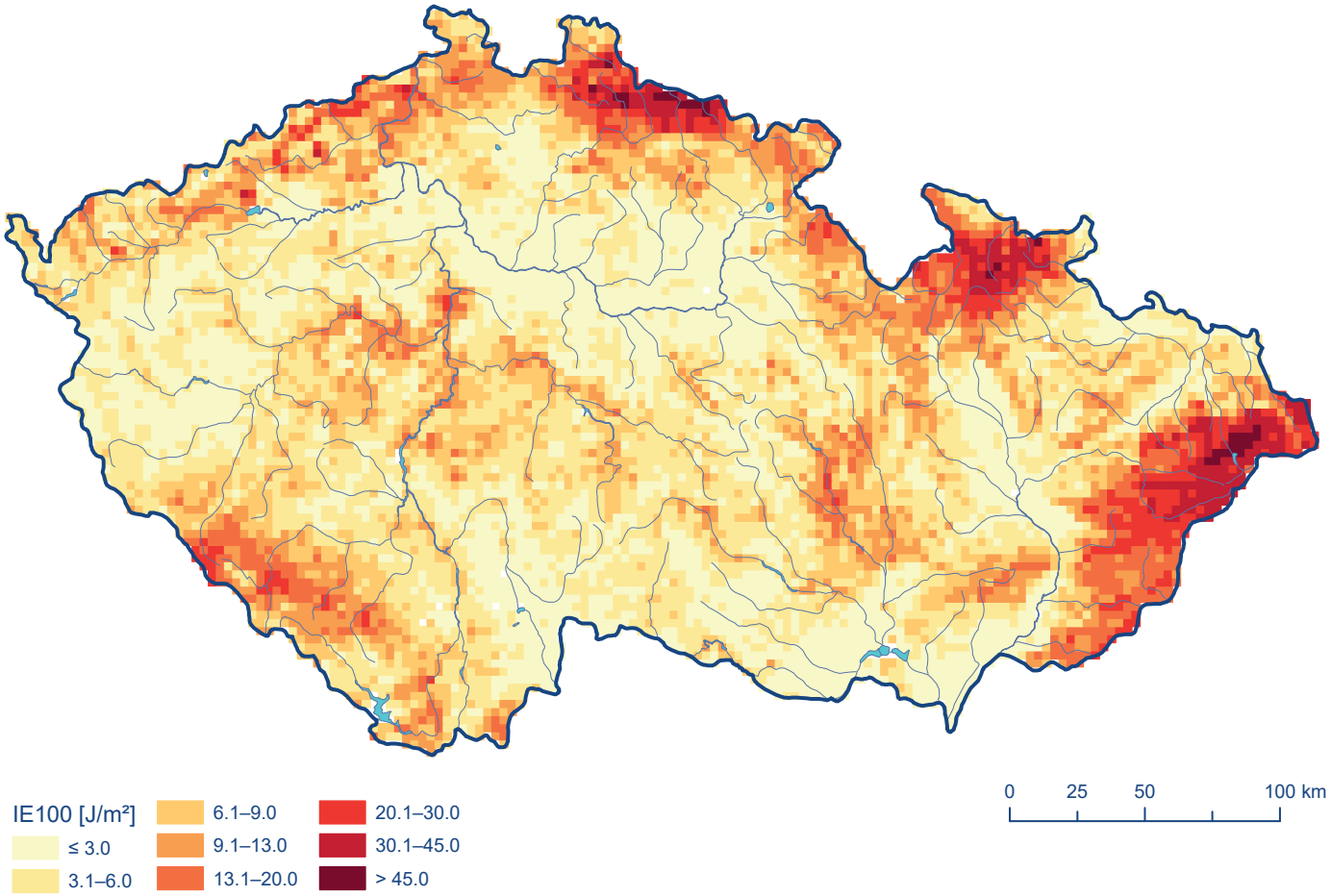

Fig. 4.5 IE_{100} values represented in a grid with a cell size of 9 km².

For the purposes of determining the flash flood risk, the procedure derived in a study by Šercl (2009) is used. The procedure to estimate q_{100} is based on the application of the so-called Extremity Index, which is the value integrating the relevant physical-geographical characteristics influencing the runoff due to extreme rainfall.

The Extremity Index IE_{100} is derived using the formula:

$$IE_{100} = \frac{1}{2} \cdot M_{100} \cdot V^2 \ [\mathrm{J \cdot m^{-2}}], \qquad (4.13)$$

where

M_{100} is the effective rain mass of 100-year 1-day rainfall [kg·m^{-2}],

V is a specific quantity representing the mean velocity of water flowing in the catchment [m·s^{-1}].

The determination of M_{100} is based on the derivation of effective rainfall R_{1001d} according to the 100-year 1-day rainfall (i.e., daily rainfall total having a return period of 100 years) P_{1001d} by the CN method and the conversion of the given volume to the mass (numerically $M_{100} \approx R_{1001d}$) using the CN_{II} values.

To determine V, the following formula is used:

$$V = \frac{L_u}{TC \cdot 3600}, \qquad (4.14)$$

where

L_u is the maximum flow length from the furthest point of the basin to the outlet [m],

TC is the Time of Concentration [h], determined according to the formula:

$$TC = 1.67 \cdot T_{LAG}, \qquad (4.15)$$

where

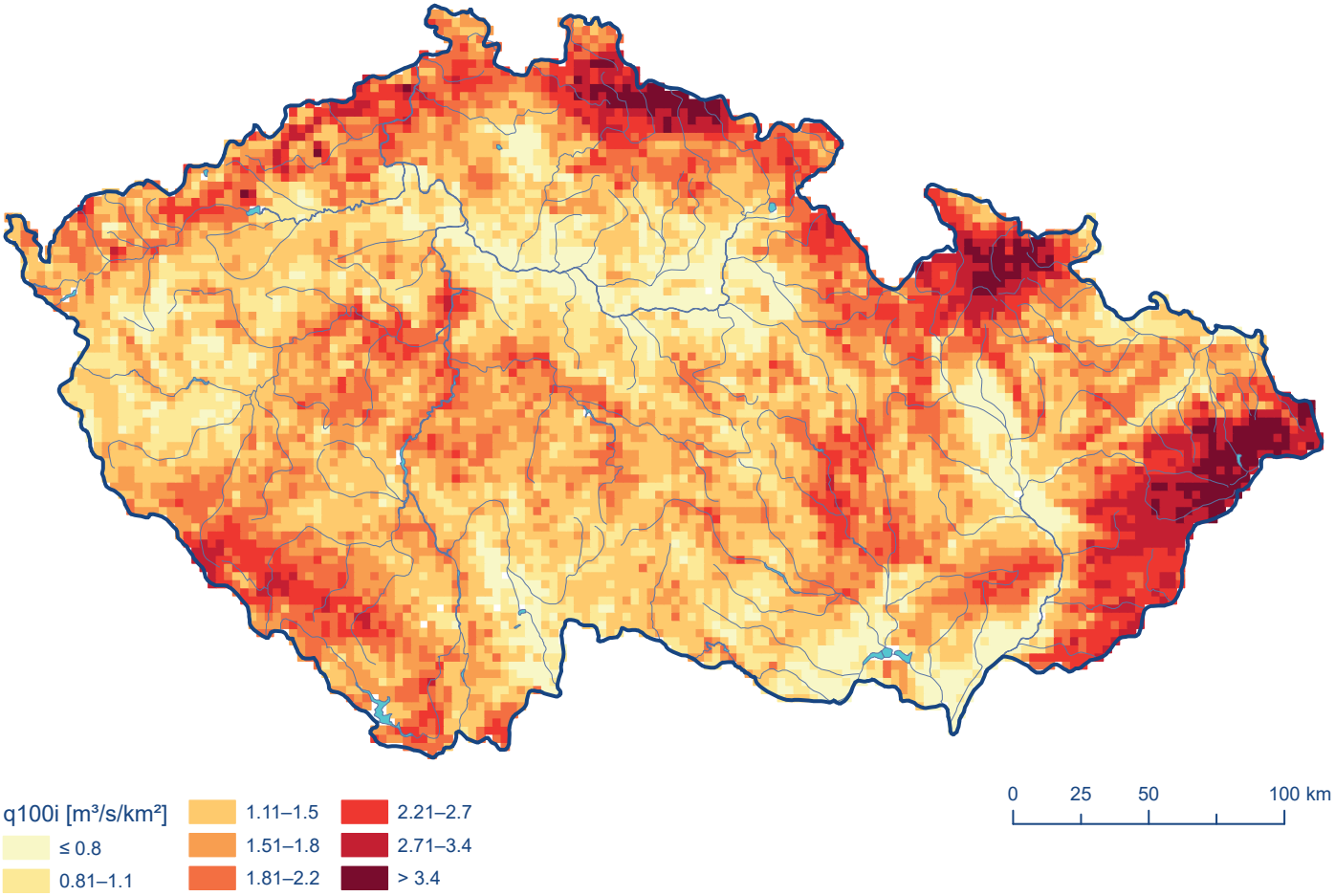

Fig. 4.6 q_{100i} values represented in a grid with a cell size of 9 km².

T_{LAG} is defined as the time difference from the centroid of the net rainfall[2] to the peak discharge at the catchment outlet. The following empirical equation was used for the calculation:

$$T_{LAG} = \frac{3.281 \cdot L_u^{0.8} \cdot (0.0394 \cdot A + 1)^{0.7}}{1900 \cdot \sqrt{Y}}, \qquad (4.16)$$

where

Y is the average catchment slope in percent.

The relationship between TC and T_{LAG} is explained in the USDA Methodology (https://directives.sc.egov.usda.gov/viewerFS.aspx?hid=21422); Chapter 15 – Time of Concentration, p. 15-3 (verified on 6 December 2022).

Figure 4.5 shows the spatial distribution of IE_{100} values as a grid[3] with a cell size of 9 km², where the calculation of potentially dangerous rainfall is taken into account (see Chapter 4.2.2). Obviously, the highest values are in areas with high slope (mountainous areas) and areas with reduced soil infiltration capacity (flysch areas, urban areas of large cities). Hence, there is a higher flash flood risk in these areas.

The 100-year specific runoff (q_{100i}) is then estimated from the following relationship:

$$q_{100i} = b_1 \cdot IE_{100}^{b_2} \cdot CA^n \ [\mathrm{m^3 \cdot s^{-1} \cdot km^{-2}}], \qquad (4.17)$$

where

2 Portion of rainfall which reaches a stream channel or the concentration point as direct surface flow.

3 The grid, and not the catchment as an areal unit, has been chosen to make the index extremity values in the map easily comparable.

b_1, b_2, and n are parameters of the regression relation,

CA is the catchment area [km^2],

IE_{100} is the Extremity Index [J·m^{-2}].

Regression coefficients b_1, b_2, and n in Equation (4.17) were derived on the basis of physical-geographical characteristics of 46 gauged basins having drainage areas less than 200 km^2, where their 100-year specific runoff mostly results (except for mountainous areas) from heavy rainfall. The coefficients were verified on 20 gauging stations.

Equation (4.17) has a coefficient of determination of 0.792, with its regression coefficient and exponents being $b_1 = 2.431$, $b_2 = 0.405$, and $n = -0.498$. The spatial distribution of q_{100i} values in a form of a grid with a cell size of 9 km^2 is shown in Fig. 4.6.

4.2.2 Calculation of potential dangerous rainfall of a given duration

The inspiration for addressing this issue was undoubtedly the 'Flash Flood Guidance System' (FFGS), which is operated by the NWS. The term 'Flash Flood Guidance' (FFG) is the sum of rainfall of a certain duration that causes flooding in local streams. The magnitude of the critical rainfall is primarily dependent on the antecedent soil moisture conditions of the area based on previous rainfall. FFG values for durations of one, three and six hours are updated daily. However, the method of determining these data is not very clear from the publication (Sweeney 1992).

Further improvements in determining the magnitude of the potential dangerous rainfall leading to a flash flood is very difficult. The problem lies mainly in the determination of the lower limit (threshold) of the rainfall intensity that results in runoff causing potential damage.

It is obvious that, in addition to the antecedent soil moisture conditions, the morphology of the terrain and the land use pattern will be important factors influencing flash flood events. Another important fact is that the flash flood is not limited to the surroundings of small watercourses alone, but may also occur in valleys that remain dry most of the year, or in areas having steeper slopes that may be affected by torrential rainfall.

The original intention was to calculate the potential dangerous rainfall for hydrological basins. As these basins differ considerably in size (from about 0.5 to 30 km^2), due to different physical-geographical characteristics (e.g., lengths of valleys), there is some inhomogeneity in estimating the flash flood risk. To avoid this, the calculation has been designed in a way largely removing the influence of the basin size, namely by employing a grid with a cell having an edge length of 3 km.

These cells (or squares) in the calculations thus act as hypothetical 'catchment areas' with a uniform area of 9 km^2, for which the physical-geographical characteristics are expressed by average values over each given location having its specific slope, altitude, CN_{II}, 100-year 1-day rainfall, 100-year 1-day runoff, etc. The length of the 'valley' was set uniformly at 3,000 meters. The Extremity Index IE_{100} and the 100-year specific runoff q_{100i} correspond to the above-mentioned characteristics for each individual grid cell. The total number of cells, which cover the Czech territory, is 8,717.

A value of 25% of q_{100i} (in this case 25% of IE_{100}) was chosen as the threshold. This level corresponds approximately to 2 to 5-year return period and is also a parameter (attribute of a specific grid cell) that can be modified based on performance assessment.

The basic task is, therefore, to determine the rainfall total of a given duration (in our case 1, 3 and 6 hours), which theoretically causes a peak flow at the level of 25% of q_{100i}. The calculation itself takes place in three following steps.

1. Loading the layer of actual CN values and calculating their averages for each individual cell.
2. Calculation of T_{LAG} [h] for each cell (see Eq. 4.16).
3. Determining the threshold peak flow and calculation of the corresponding rainfall depth using the SCS unit hydrograph method.

$$Q_{tr} = tr \cdot q_{100i} \cdot CA, \qquad (4.18)$$

where

Q_{tr} is the overall peak flow [m^3·s^{-1}],

tr is the ratio to the specific runoff reference value of 0.25,

q_{100i} is the 100-year specific runoff [m^3·s^{-1}·km^{-2}] obtained from Eq. (4.13) and Eq. (4.17),

CA is the area of the grid cell [km^2], in our case 9 km^2.

The flood volume is obtained from the schematic triangular shape of the flood hydrograph, where the base is the sum of the rise time (t_p) and the fall time (t_{re}) and the height is the overall peak flow Q_{tr} (from the application of the SCS method):

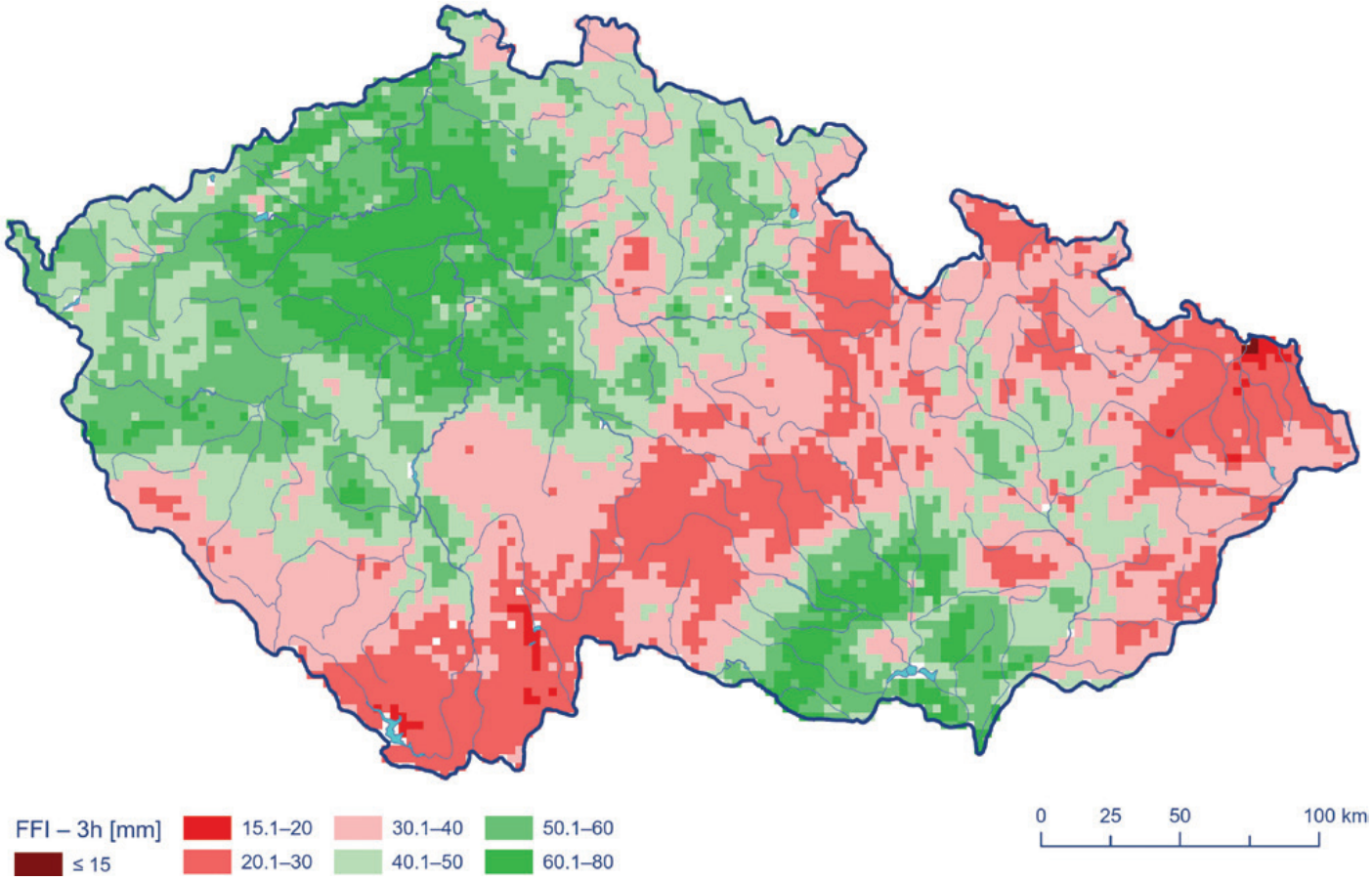

Fig. 4.7 Example of the areal distribution of potential dangerous rainfall for duration of 3 hours valid for July 19, 2020 at 06:00 UTC.

$$t_p = T_{LAG} + \frac{D}{2}, \tag{4.19}$$

$$t_{re} = t_p \cdot 1.67, \tag{4.20}$$

$$W_D = \frac{1}{2} \cdot \left(Q_{tr} \cdot \left((t_p + t_{re}) \cdot 3600 \right) \right), \tag{4.21}$$

where

W_D is the volume of the schematized flood hydrograph [m³],

$$R_D = \frac{W_D}{A \cdot 1000}, \tag{4.22}$$

where

R_D is the runoff depth [mm],

D is the duration of the critical rainfall [h].

The *CN* method is then used to derive the magnitude of the rainfall in mm from the 'known' direct runoff value.

Figure 4.7 shows an example of the output from a potential risk-inducing rainfall of duration D = 3 hours for July 19, 2020 at 06:00 UTC.

4.3 Determining the actual flash flood risk in a river basin system

The calculation is based on a well-defined scheme of hydrologically oriented elements (in the direction of flow), which form individual sub-catchments and river reaches.

For all river sub-catchments that were considered, the following physical-geographical characteristics were derived in GIS:

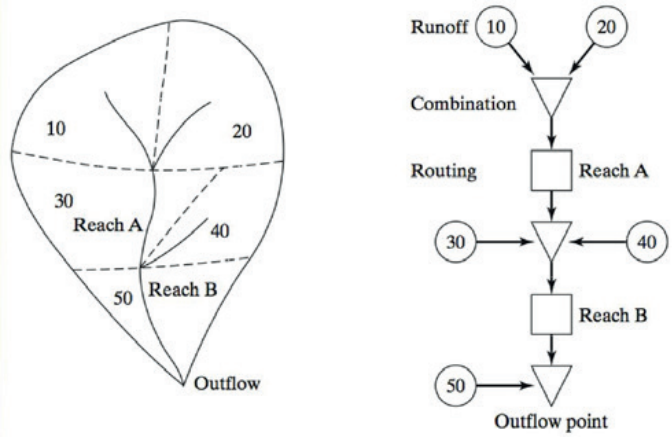

Fig. 4.8 Catchments and river reaches model configuration.

– catchment area *CA* [km²],

– average slope of the catchment *Y* [-],

– distance from the catchment outlet to the hydraulically furthest point from the outlet (length of the longest flow path in the catchment) L_u [km],

– slope of the longest flow path between 10% and 85% of its length S_{1085} [-],

– length of flow section L_t [km],

– Extremity Index IE_{100},

– IE_{100r} – corrected Extremity Index, determined as a weighted average (according to every sub-catchment area) of the IE_{100} values for all sub-catchments lying upstream.

In the scheme, sub-catchments are distinguished either as upper (catchments 10, 20, 40; see Fig. 4.8) or lower with river reaches (catchment 30 and reach A, catchment 50 and reach B). The lower catchment area can also be understood as an inter-catchment.

The area of 120 km² (subject to change) is considered the maximum river basin size (total area of upper and lower catchments) for which IE_{100r} is calculated and for which the flash flood risk estimation is applied. There are 6,916 catchments (could be changed) in FFI with area from several hectares to 30 km² (in average 9 km²), which are hydrologically connected. The total number of gauging stations with a catchment area of 120 km² or less is roughly 300, which means they cover only small part from all catchments involved.

In the downstream catchments, in addition to the actual hydrological response calculation (hydrograph), the estimation of the travel time and flow transformation in the river reach is also performed (river routing).

The basic input to the calculation includes:

– average rainfall depth from adjusted radar QPEs for all considered catchments in the form of a hyetograph in the defined time step (15 minutes, subject to change), while the period of 3 hours before the individual model run and 30 minutes (subject to change) of nowcasting is used, and

– updated *CN* values derived from the water balance calculations described in Chapter 4.1, in the form of average values for all considered catchments.

The calculation procedure can be divided into the following steps:

– 15-minute rainfall depths are transformed into runoff depths (rainfall excess) using the *CN* method described in Chapter 4.1.

– The hydrological response is calculated for individual catchments in the form of discharge time series using the selected unit hydrograph method (SCS or Clark).

– In downstream sub-catchments, the river routing of the inflow hydrograph(s) from upstream catchment(s) is applied (Muskingum), and the resulting overall hydrograph is calculated as the sum of the ordinates of the hydrological response of the particular catchment and the routed hydrograph.

– Finally, estimated peak flow values in the catchment outlets are compared to the defined thresholds (selected ratios to q_{100i} are used).

4.3.1 Calculation of runoff response

The unit hydrograph methods according to Clark and SCS were chosen to estimate the stream's hydrological response. While the SCS method uses a single parameter, the so-called T_{LAG} (time delay, in hours, between the moment of the maximum rainfall and the moment of the occurrence of the peak flow in the catchment), the Clark unit hydrograph method uses two (or three) parameters:

– *TC* – time of concentration [h],

– *R* – transforming factor [h] reflecting the retention time of water in the catchment (storage coefficient),

– Time-area curve describing dependence of the response time on the size of the catchment area.

Several formulas are available to estimate the *TC* value, see Dingman (2002). Our solution uses the SCS formula (Soil

Conservation Service in the USA, now called the USDA), to derive the T_{LAG}, see Equation (4.16).

The time of concentration, TC, is then estimated from Eq. (4.15).

As is apparent from Equation (4.16), the value of T_{LAG}, and hence the value of TC, are not constant but vary with respect to the current value of CN, which determines the maximum retention of the catchment by Equation (4.2).

There are only few ways of estimating a transforming factor R. It is usually estimated as n times the time of concentration:

$$R = n \cdot TC \text{ [h]}, \tag{4.23}$$

where the value of n is mostly in the range of 1.2 to 2.

Based on available literature (Straub et al. 2000), another formula for calculating R is:

$$R = a \cdot L_u^b \cdot 3274 \cdot S_{1085}^c, \tag{4.24}$$

where

S_{1085} is the slope of the longest flow path between 10% and 85% of its length [-],

a, b, c are the parameters that were originally derived by the State of Illinois in the USA (Straub et al. 2000).

The Equation (4.24) is more sophisticated than Equation (4.23), because it involves reliance on the physical geographic characteristics of a particular catchment, therefore it was used to estimate the transforming factor R.

Based on simulated calculations of flood events in Czechia, the parameters of Equation (4.24) were found to be $a = 80$, $b = 0.342$, $c = -0.79$.

In contrast to the T_{LAG} (or TC) values, the value of the transforming factor R can be considered constant over time, since the length and slope of the valley are geomorphological characteristics that only change with geological and geomorphological processes.

Dependence of the response time on the catchment area (i.e., time-area curve) is calculated from the formulas:

$$\frac{CA_t}{CA} = 1.414 \cdot \left(\frac{t}{TC}\right)^{1.5}, \text{ if } t \leq 0.5 \cdot TC, \tag{4.25}$$

$$\frac{CA_t}{CA} = 1 - 1.414 \cdot \left(1 - \frac{t}{TC}\right)^{1.5}, \text{ if } t > 0.5 \cdot TC, \tag{4.26}$$

where

CA_t is the catchment area contributing to runoff at time t [km^2],

CA is the total catchment area [km^2].

The runoff responses are always calculated for individual hyetographs of effective rainfall (5 minutes in our case) and the resulting hydrograph is determined by convoluting partial hydrographs. Detailed description of runoff response calculation according to the Clark and SCS methodologies is provided in (USACE 1994).

4.3.2 Wave routing

The Muskingum method was used for the hydrograph routing. It is thoroughly described in the literature, see USACE (1994), and is based on a simple water balance at the inlet and outlet of the river reach:

$$S = K \cdot [XI + (1 - X) \cdot O], \tag{4.27}$$

where

S is the volume of water retained in the river reach [m^3],

O is the average runoff from the river reach [m^3·s^{-1}],

I is the average inflow into the river reach [m^3·s^{-1}],

K is the time of wave progression for the given river reach [h],

X is the transformation factor [-].

The method has two parameters K and X which must be estimated. The parameter X takes values from 0 to 0.5, where the value 0.5 represents the zero transformation and the value 0 represents the maximum transformation. For determining the parameter K, it is necessary to estimate the velocity of the wave in the given river reach and its known length.

Empirical relations were proposed for estimating the parameters X and K:

$$X = 0.5 \cdot \frac{S_{1085} - S_{1085\min}}{(S_{1085\max} - S_{1085\min})^{n_X}}, \tag{4.28}$$

$$K = \frac{L_t}{V \cdot n_K \cdot 3.6}, \tag{4.29}$$

where

S_{1085} is the value of S_{1085} in the basin,

$S_{1085min}$ is the minimum value of S_{1085} found in Czechia,

$S_{1085max}$ is the maximum value of S_{1085} found in Czechia,

n_X is a coefficient considered to be equal to 1/3,

L_t is the length of the stream in the river reach [km],

V is a value of velocity [m·s^{-1}] obtained from Equation (4.14),

n_K is the coefficient considered to have a value of 3.

Based on experience, the value of the parameter K has significantly greater effect on the overall result of the routing procedure than parameter X. The values of the coefficients n_X and n_K were estimated based on an analysis of the disastrous flash flood of July 2002 at the Hodonínka Stream (left tributary of the Svratka River) in Blansko, where the flows were evaluated in several profiles of the main stream as well as of tributaries (Soukalová 2002).

4.3.3 Criterion for determining the level of the flash flood risk

During the calculation process, catchments are eliminated for which the criterion for flash flood risk warning is most likely not met. This criterion is set as a ratio (set at 0.1) of the value of current extremity index relative to the extremity index IE_{100}. The actual extremity index is calculated according to Equation (4.13), but in the equation, the values of runoff and velocity are used according to the current state of catchment saturation.

For remaining catchments, the calculation is performed according to the approach mentioned above. The value of the maximum specific q_{maxi} runoff in the river basin profiles is compared to the specific runoff values q_{100i}, based on their multiplication by threshold ratios (r_1, r_2 and r_3), and the level of the flash flood risk is determined, see Tab. 4.2.

4.4 Determination of the risk of local flooding in a grid

The procedure is likewise applied to the polygon layer of a regular square of 3×3 km size; the structure, including attributes, is described in Chapter 4.2.2.

The disadvantage of this approach is the hydrological discontinuity resulting from the characteristics of the input layer (individual squares are not hydraulically connected), so the assessment of the risk is derived from only the rainfall that has occurred (or potentially will occur) on a specific area delimited by the polygon.

On the contrary, the advantage lies in the fact that the calculations are carried out on areas of a uniform size, and the probability is determined for the whole area of Czechia, including the areas surrounding the large watercourses, where pluvial flooding might occur with significant consequences.

The calculation itself is much simpler than the approach described in Chapter 4.3. It uses the current soil moisture conditions of the area given by the CN values for each square. According to Equation (4.17), the T_{LAG} parameter is determined from the physical-geographical characteristics, and the maximum specific runoff is determined by the SCS unit hydrograph method.

The rainfall input is in the form of 2-hour total of adjusted radar QPEs as an average for each square (grid), utilizing two methods. In the first method, the rainfall input is taken as a total of the rainfall that occurred in previous 2 hours.

Tab. 4.2 Description of the warning levels for flash flood risk and their threshold ratios.

Risk level		Description	Threshold ratio (r_i) in 2021
1	Low to medium risk	High rise of water level, the flow stays in river bed, public should stay informed about situation	0.15
2	High risk	Flow gets out of river bed locally, there are not significant damages, public should pay increased attention and try to protect its property	0.40
3	Very high risk	Flow gets out of river bed in many places, there are significant damages on property, possible loss of life, public should be prepared for evacuation	0.80

Tab. 4.3 Description of the warning levels for local flooding risk and their threshold ratios.

Risk level		Description	Threshold ratio (r_i) in 2021
1	Low to medium risk	Concentrated surface runoff begins to form outside the river beds, flooding may already occur in the lowest places, most of the time there is no damage to property, public should stay informed about situation.	0.25
2	High risk	There is a concentrated surface runoff, lower places are flooded, but most of the time there is no significant damage to property, but residents should keep a close eye on the development of the situation and try to protect their property.	0.60
3	Very high risk	There is a significantly concentrated surface runoff, extensive flooding at lower places, significant damage to property and potential risk of fatalities, residents should not put themselves at risk and stay as far as possible in safe places.	0.95

In the second method, the rainfall total is taken as the sum of rainfall that occurred in previous 60 minutes and the amount of rainfall predicted for the next 60 minutes (from nowcasting). The results are evaluated separately for both methods, and the result showing a higher potential risk is considered the resulting risk of local flooding for each square (grid).

The value of the maximum specific runoff q_{maxi} for each grid cell is compared to the specific runoff values q_{100i}, based on the threshold ratios (r_1, r_2 and r_3) against the value of q_{100i}, and that way the level of local flooding risk is determined, see Chapter 4.3.3.

The meaning of warning levels for local flooding is similar to those described in Chapter 4.3.3 (Tab. 4.2), but the risk is primarily focused on locations, which are not near permanent watercourses, see Tab. 4.3.

The ratios r_1, r_2, r_3 in Tab. 4.2 and Tab. 4.3 were estimated empirically as constant values all over the Czechia. Their values may be changed based on experience.

5. Description of the FFI Operation

The FFI is operated from mid-April to mid-October. It is the time of the year when one usually expects significant convective precipitation and subsequent flash floods on Czechia's territory.

The FFI system can be run either interactively (from the GIS environment) or automatically, using a task scheduler in the operating system. Based on the auto-start interval, the FFI procedures can be operated in the following ways:

– run in a daily time step,
– run in a shorter time step (by configuration).

In the daily step, the output is produced in the following GIS layers:

– up-to-date data on the soil moisture conditions of the area (represented by *CN* values), derived from the daily time step of the water balance of the daily rainfall, runoff and evapotranspiration, where the main output is the so-called soil saturation indicator (for description, see Chapter 4.1),

– potential dangerous rainfall amounts of a given duration (1, 3, and 6 hours) for grids with the cell size of 9 km^2 (for description, see Chapter 4.2).

For each of the above procedures, configuration files are available. These files contain many parameters users can set up, e.g., the paths to input data and the names of folders to store the results, computing time step, q_{100i} threshold ratios to for determining individual risk levels, and many others.

These calculations are run several times a day (usually three times), in order to be able to correct possible errors in the input data and recalculate the results with the corrected inputs (what applies mostly to rainfall).

The system launch in shorter, user-defined, step includes comprehensive procedure ensuring the import of radar QPEs (including nowcasting) and calculation of runoff response at the corresponding individual catchments through a network of hydrologically connected elements of the river basin and river reaches. For each individual catchment, imminent flash flood risk level is computed (Chapter 4.3).

After the completion of the above procedure, the calculation of the risk level of local flooding in the grids with the cell size of 9 km^2 is started (Chapter 4.4).

As the main result, the level of local flooding risk and flash flood risk is determined for each municipality with extended powers (MEP)[4]. District responsibilities are among others clearly defined in the field of flood management.

The combination of the computed level of the risk of local flooding and the level of the flash flood risk in catchments is applied to set a general risk for each MEP, see Tab. 5.1.

If an imminent risk of flood is detected, warnings are generated in the following formats:

– structured XML file with the information about the flash flood risk for particular MEPs; this file can be used, e.g., as an input to the CHMI mobile application,

– plain text file with the information about the flash flood risk in particular catchments and corresponding MEPs,

– plain text file with the information about the risk of local flooding in corresponding MEPs.

All outputs are stored in ESRI file geodatabases in the form of raster datasets, vector datasets or standalone tables. Selected data are then transferred to the cloud storage on ArcGIS Online and displayed in the form of web maps and through interactive web mapping applications.

Tab. 5.1 Matrix for setting a general risk level for MEPs. Rows represent the flash flood risk, columns represent the local flooding risk.

		Local flooding risk level			
		No risk	**Medium risk**	**High risk**	**Very high risk**
Flash flood risk level	**No risk**	No risk	Medium risk	Medium risk	High risk
	Medium risk	Medium risk	Medium risk	Medium risk	High risk
	High risk	Medium risk	High risk	High risk	High risk
	Very high risk	High risk	Very high risk	Very high risk	Very high risk

4 There's a four level organization of autonomous public government: national, 14 regions, 205 municipalities with extended powers (MEP), and approx. 6000 local municipalities.

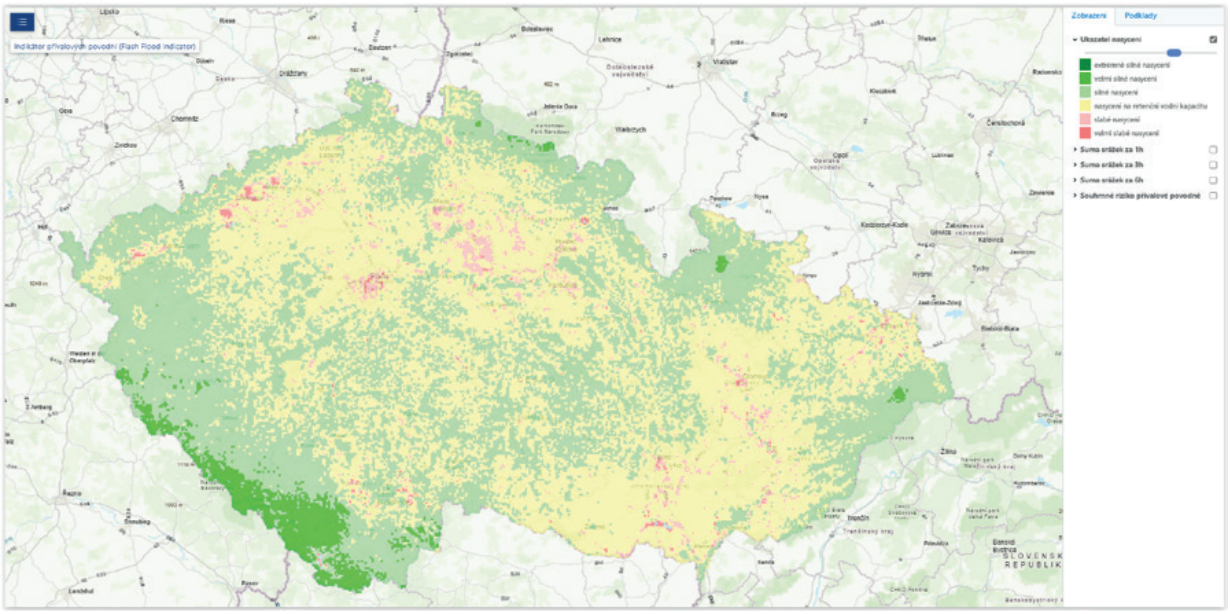

Fig. 5.1 Soil saturation indicator map valid for May 13, 2023 at 06:00 UTC as presented on the CHMI website. For map legend translation, see Tab. 4.1.

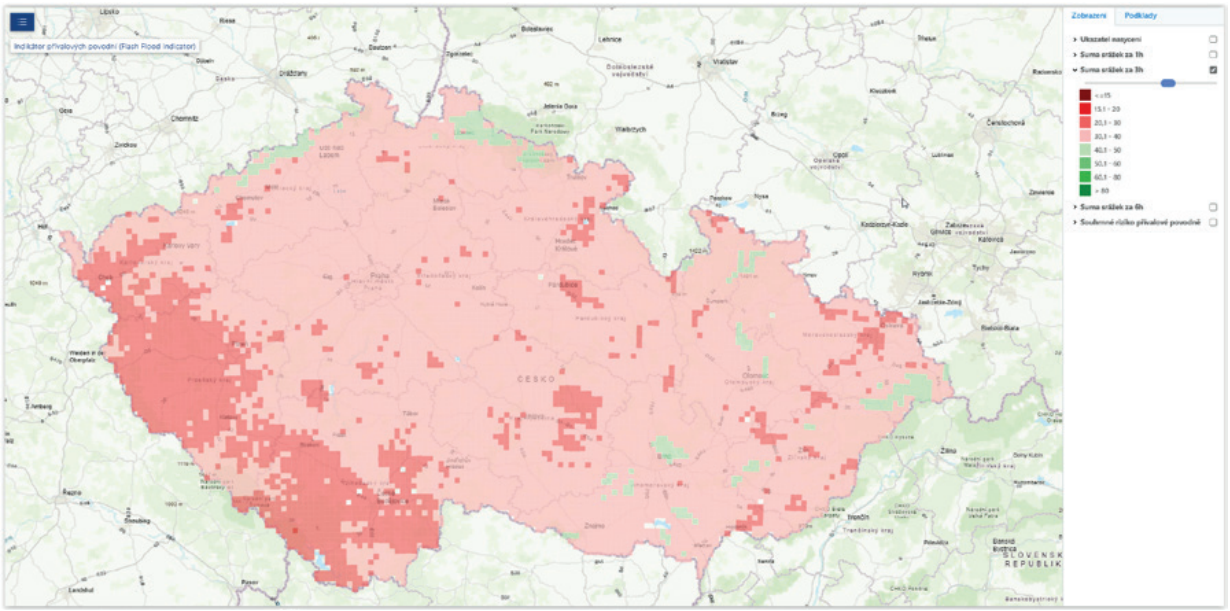

Fig. 5.2 Map of potential dangerous rainfall amounts with the duration of 3 hours valid for May 13, 2023 at 06:00 UTC as presented on the CHMI website.

The following two figures (Fig. 5.1 and 5.2) show the web maps that are presented on the CHMI website.

Figure 5.1 represents a web map with a soil saturation indicator, while in Fig. 5.2, the potential dangerous precipitation with a duration of 3 hours is displayed. Both web maps are fully interactive.

Figure 5.3 illustrates the web map application in which it is possible to show all important and actual FFI system outputs:

- soil saturation indicator,
- potentially dangerous precipitation with duration of 1, 3 and 6 hours,
- local flooding risk for particular MEPs,
- flash flood risk for particular MEPs,
- general flash flood risk for particular MEPs as a combination of the local flooding risk and the flash flood risk (see above in this chapter),

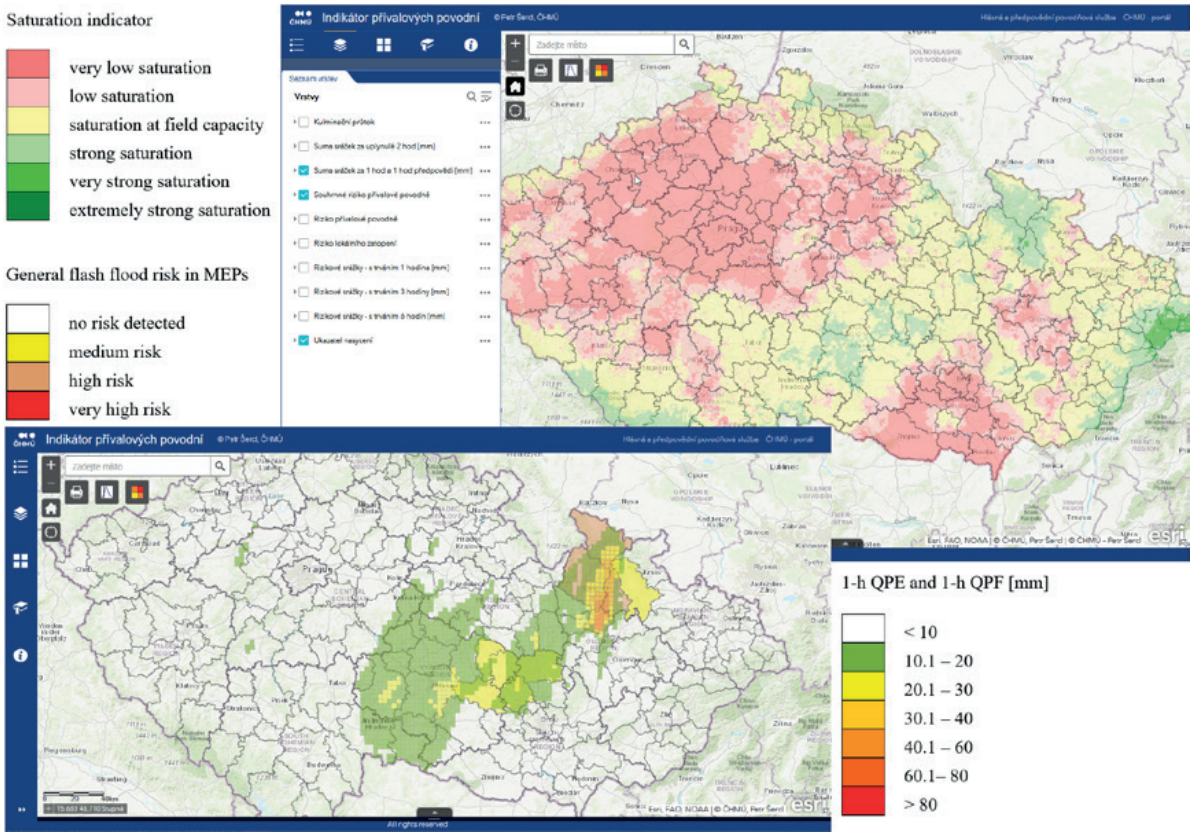

Fig. 5.3 The outputs from web map application 'Flash Flood Indicator' running on the ArcGIS Online platform. It depicts the soil saturation indicator layer (upper-right), precipitation amounts ≥ 10 mm/2h overlaid on general flash flood risk for affected MEPs (bottom left).

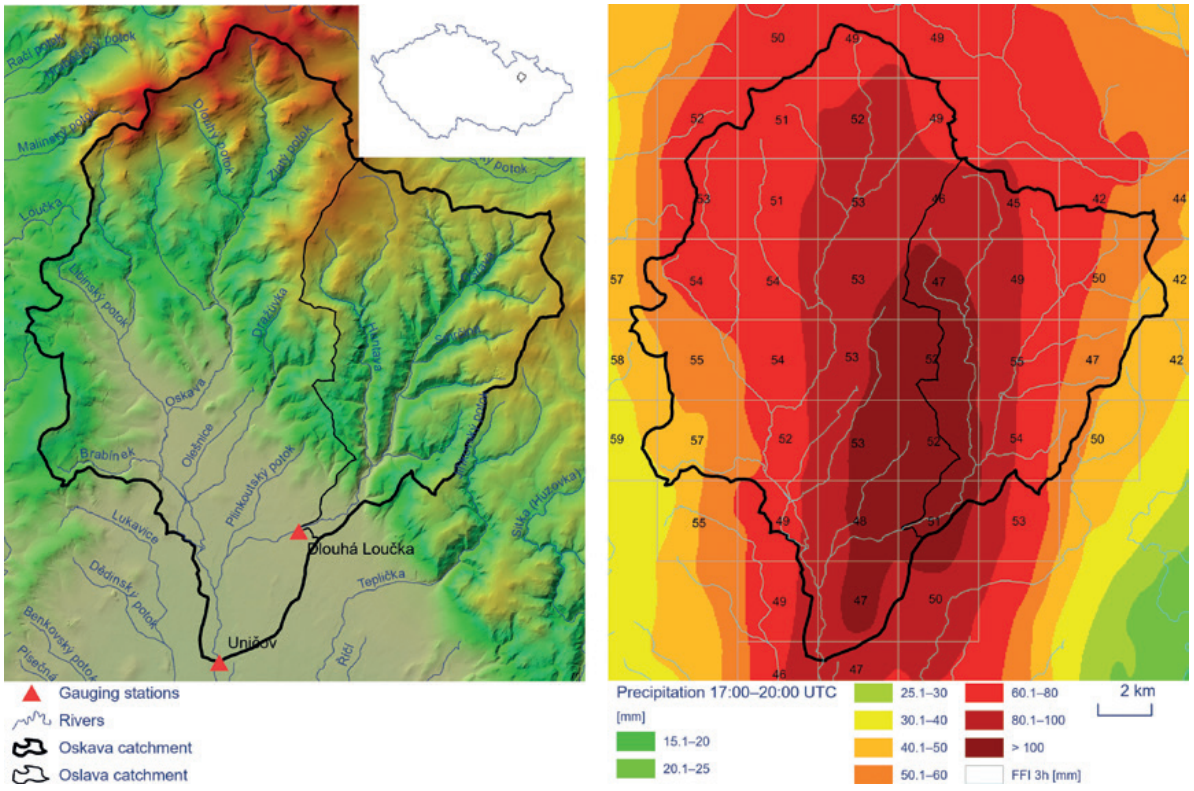

Fig. 5.4 Physical-geographical characteristics of the Oskava basin (left). Adjusted radar QPE for June 7, 2020 17:00–20:00 UTC and potential dangerous precipitation for the duration of 3 hours (right) for June 7, 2020 at 06:00 UTC.

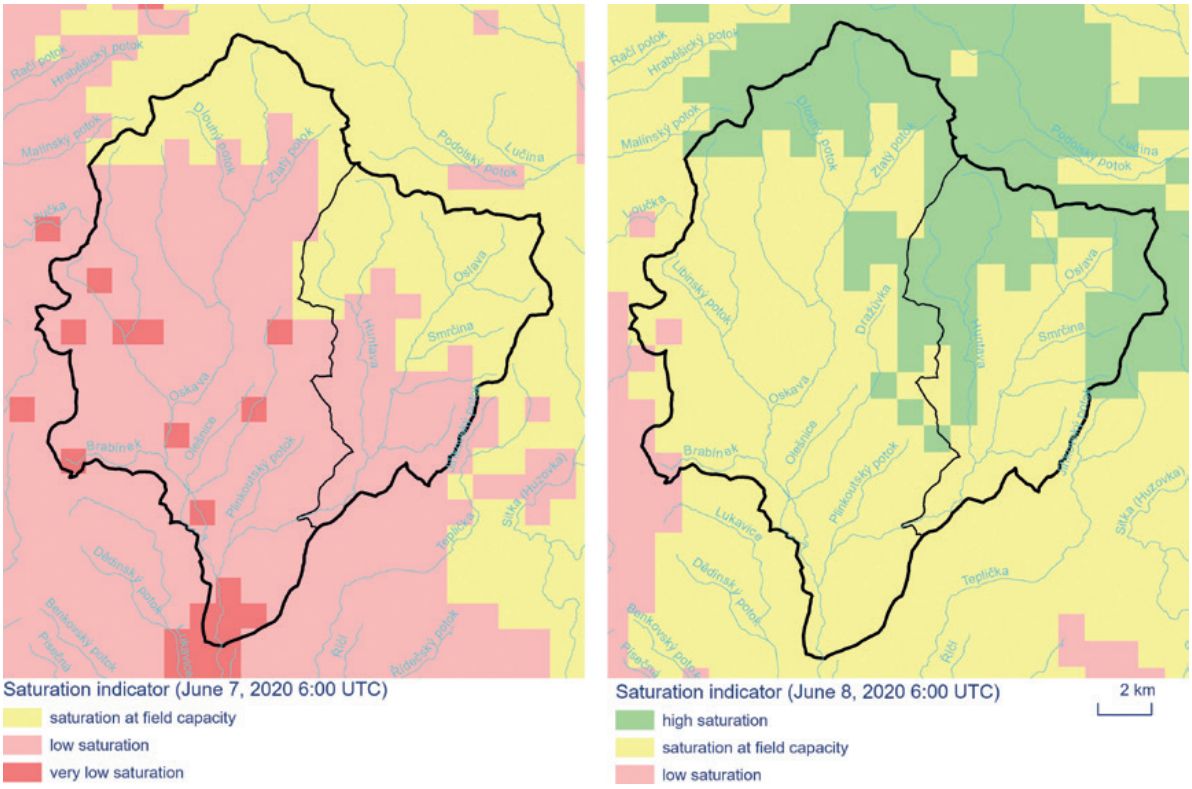

Fig. 5.5 The saturation indicator valid for June 7, 2020 at 06:00 UTC (left) and the saturation indicator valid for June 8, 2020 at 06:00 UTC (right).

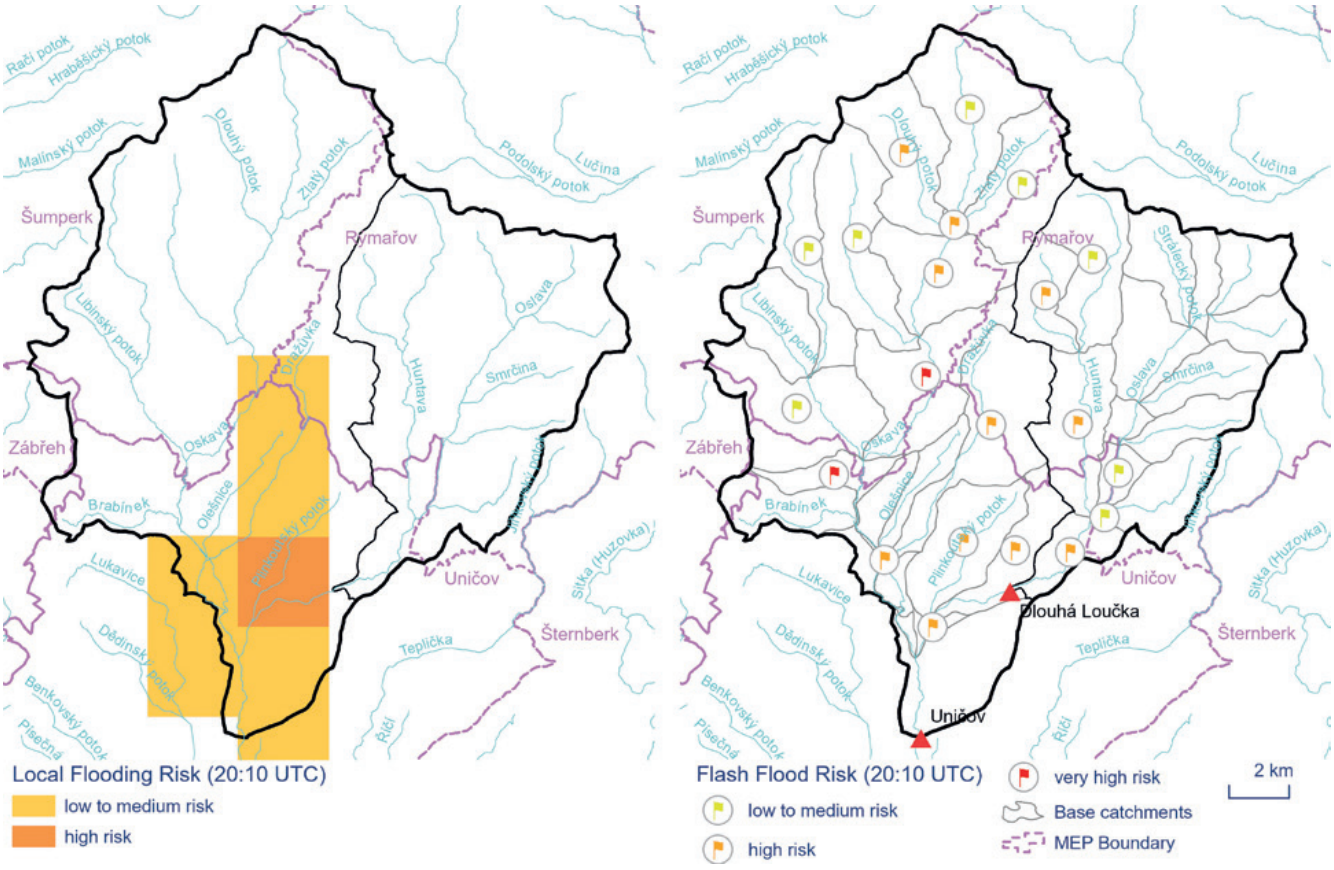

Fig. 5.6 Local flooding risk (left) and flash flood risk (right) for June 7, 2020 at 20:10 UTC.

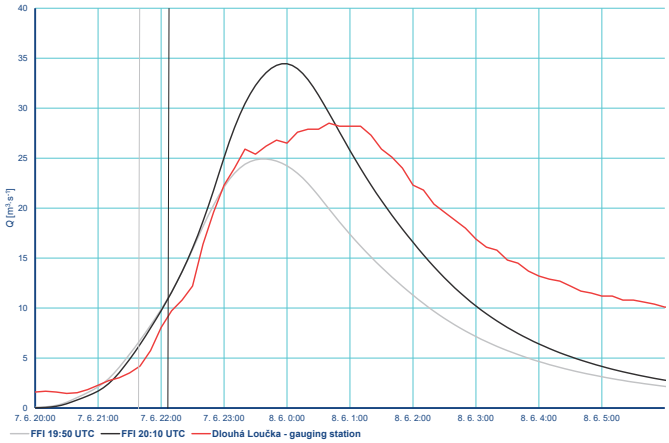

Fig. 5.7 Observed and forecasted hydrographs at the Dlouhá Loučka water-gauging station. The X-axis presents the local time (CET).

– sum of adjusted radar QPEs in the grids of resolution 3×3 km during previous 2 hours, if the sum was higher than 10 mm or if this sum represented a risk of local flooding,

– sum of adjusted radar QPEs in the grids of resolution 3×3 km for the previous hour plus the hour ahead taken from nowcasting, if the sum is higher than 10 mm or if this sum represents a risk of local flooding,

– flash flood risk in the river basin system, where, in addition to indicated level of risk, time of the peak flow can be displayed[5] with the possibility to filter the catchments where the peak flow is being expected.

A detailed FFI outputs for a particular flood event that occurred on June 7, 2020 in the north of Moravia in the Oskava River basin are presented. The Oskava River is a left tributary of the Morava River.

The flood was caused by torrential rainfall that had occurred over the area for about three hours. The thunderstorms were advancing from south to north, arranged in so called train effect. The runoff response was very rapid and accompanied by debris flow. Property damage was considerable, and, unfortunately, there were also two fatalities reported.

There are two water gauging stations in the Oskava River basin. Dlouhá Loučka water gauge (Oslava Stream; catchment area 80.8 km²) recorded the peak flow with a return period of 50 years. At a downstream laying Uničov water gauge (Oskava River; catchment area 256.26 km²), the peak flow return period was significantly shorter due to flood transformation in the floodplain.

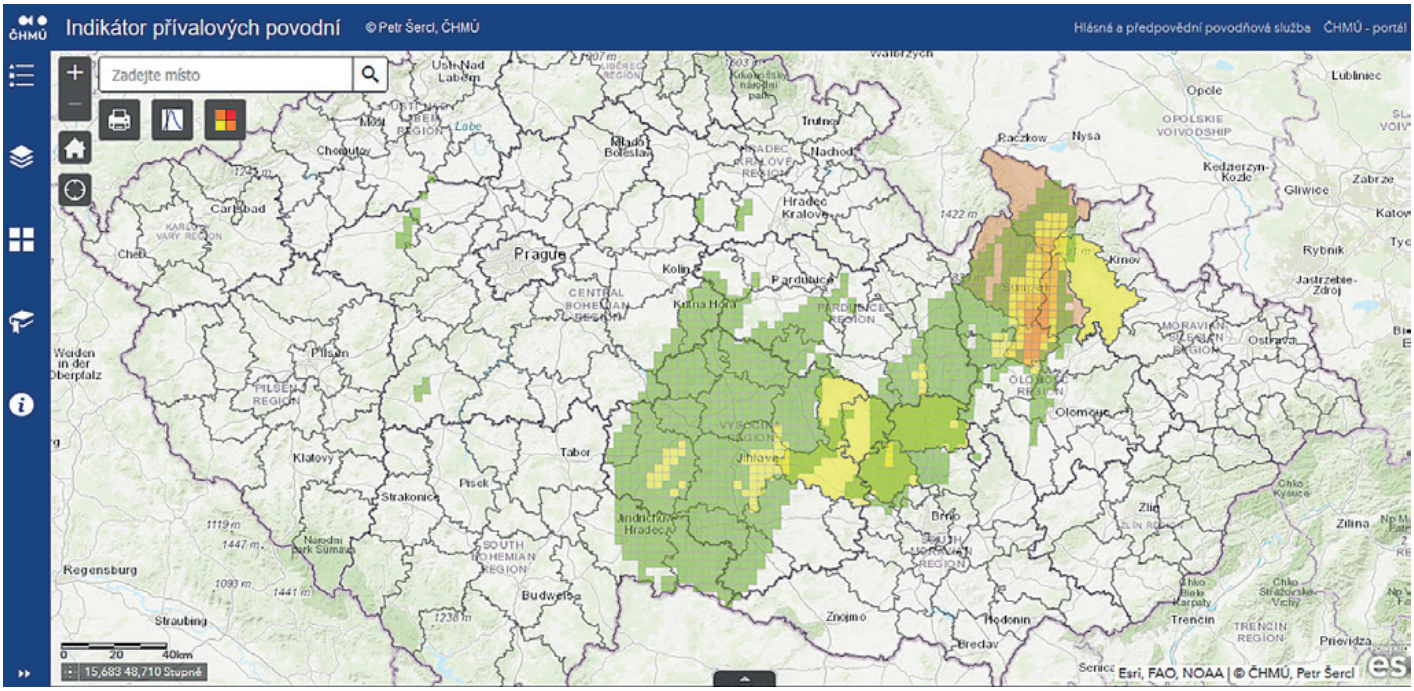

Fig. 5.8 Rainfall above 10 mm and actual risks for the MEPs in Czechia taken from the FFI application for June 8, 2020 18:30 UTC.

5 The FFI procedure, which determines the risk of a torrential flood in a system of hydrologically connected basins, calculates the whole progress of the hydrological response on individual catchments and sub-catchments.

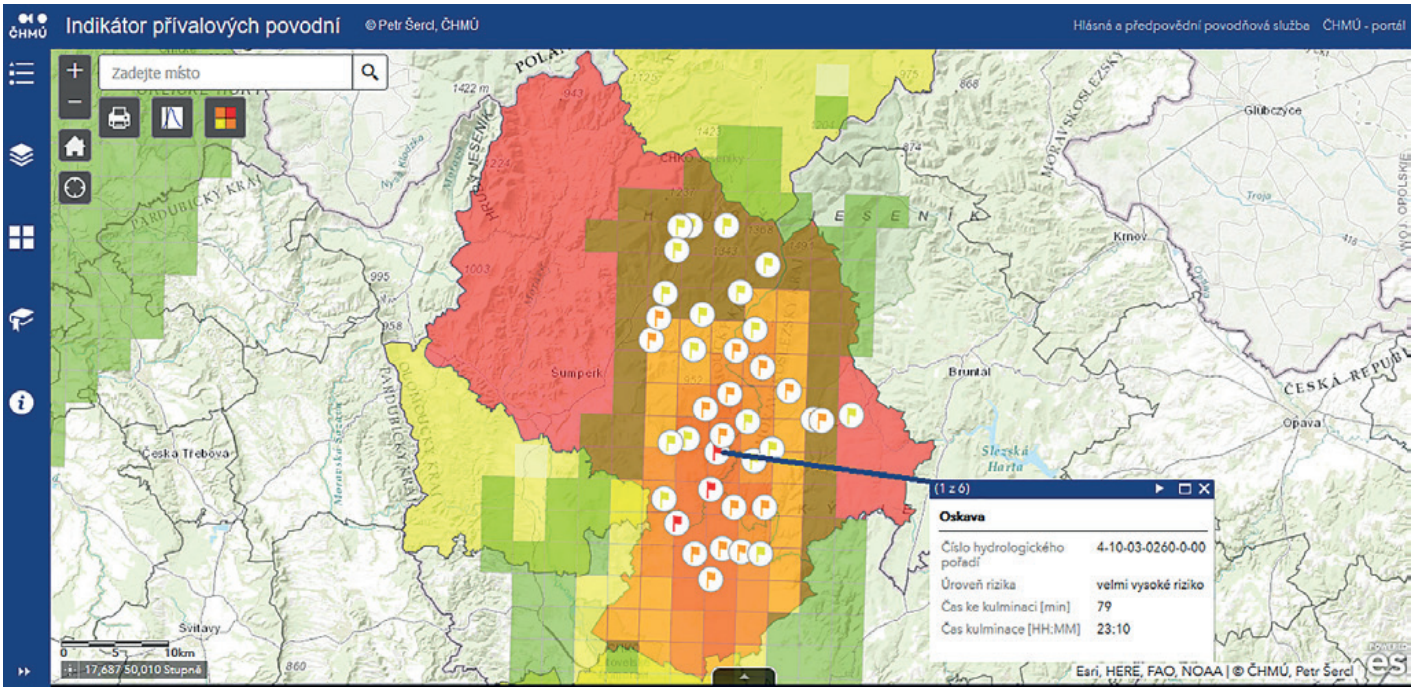

Fig. 5.9 Rainfall above 10 mm and actual risks for the MEPs and small catchments in the Uničov region taken from the FFI application for June 8, 2020 at 19:50 UTC.

Figures 5.4–5.7 show the flood situation in the Uničov region from the perspective of FFI outputs. The sum of three-hour adjusted QPEs and three-hour potential dangerous precipitation are shown in Figure 5.4 on the right. Figure 5.5 shows the saturation indicator valid before the precipitation event occurred and the saturation indicator valid on the following day.

The flash flood risk and the risk of local flooding by the 20:10 UTC are shown in Fig. 5.6. Figure 5.7 shows the hydrographs of the flood at Dlouhá Loučka water gauge calculated by FFI rainfall-runoff routine initiated at 19:50 UTC and at 20:10 UTC in comparison to observed hydrograph of the flood derived from the rating curve.

Torrential rain and the formation of a torrential flood (footage from the bus driver's cab).

The aftermath of a flash flood (footage of firefighters).

FFI procedures continuously detected the flash flood risk or the risk of local flooding on that day already during the afternoon when local intense showers and rainstorms occurred at many places. In most cases, there were only the lowest levels of the risk.

As early as 17:50 UTC, the lowest level of local flooding was estimated for the territories of the Šumperk and Rýmařov MEPs neighbouring the most affected Uničov MEP. Similar signal was obtained from 18:10 UTC calculation. For the most affected area of the Uničov region, the risk of local flooding or flash flood was first indicated by the run from 18:30 UTC (Fig. 5.8). However, in the next run at 18:50 UTC, "very high risk" of the flash flood was computed for the Oskava River catchment, and "high risk" level was identified for the Oslava and Dražůvka Streams as well as for other catchments of smaller tributaries of above mentioned rivers. From that time, each run (every 20 minutes) delivered high or very high risk of flash flood or local flooding for most watercourses in the Uničov, Rýmařov and Šumperk MEPs territories (Fig. 5.9). The warnings were issued until midnight, while their issuing stopped with weakening rainfalls and culminating watercourses in the affected area.

6. FFI Operation Experience

As already mentioned, the FFI system was put into trial operation in 2010. However, the system and its procedures were further developed and optimized during the following years. Experience from the period 2017–2020 shows that the system operation and results are reliable. Remaining problem is related to the quality of input data, in particular the adjusted radar QPEs. Another issue is the lack of real-time quality control of the data from rain gauges.

6.1 Influence of input data quality and reliability

The FFI is a rainfall-runoff model where the quality of outputs depends on the quality of inputs.

First, it is important to say that necessary input data to the system were, with some minor exceptions, supplied for processing in time. However, the quality of data represents an issue that will be described in detail further in the text.

6.1.1 QPE calculation

Areal quantitative rainfall estimate (QPE) is arguably the most important input to the FFI. These estimates are based on the combination of radar and rain gauge measurements.

In the first step, radar reflectivity measurements are converted into radar-only rainfall estimates. The radar-only estimates are based on the PseudoCAPPI 2 km radar product (radar reflectivity at the altitude of 2 km above mean sea level), which was previously identified as optimal for rainfall estimates over the territory of Czechia (Novák, Kráčmar 2001). It is close enough to the ground to be representative of the rainfall at the ground but, on the other hand, far enough not to be significantly influenced, e.g., by the terrain features or orography attenuation. The Marshall-Palmer equation in the form

$$Z = 200 \cdot R^{1.6}, \tag{6.1}$$

where

Z is the reflectivity factor in [mm6·m^{-3}], and

R is the rainfall rate in [mm·h^{-1}],

is used for conversion of the radar reflectivity into the rainfall rate. Two thresholds are applied to the converted rainfall rate values:

– if $Z < 7$ dBZ, $R = 0$ mm·h^{-1}, the threshold condition is used to eliminate weak non-precipitation echoes,

– if $Z \geq 55$ dBZ, $R = 99.85$ mm·h^{-1}, the threshold condition is applied to reduce rainfall rate overestimations caused by the occurrence of hails in convective storms.

In the next step, converted rainfall rate fields are integrated for given time periods to get the radar-only rainfall estimates. Radar measurements are updated every 5 minutes, which should be sufficient to get a realistic smooth areal rainfall estimate in most cases. Problems may occur in case of fast-moving storms when we can see periodic changes in rainfall along the storm path ('stroboscopic' effect). To eliminate this effect, radar products are interpolated into fields with a 1-minute time step using the COTREC moving vector fields (Novák 2007; Novák et al. 2009) before the QPE accumulation. In operation, rainfall accumulations (radar-only rainfall estimates) are calculated every 5 minutes for different time intervals.

Every 10 minutes, as the new rain gauge measurements are available, the advanced radar-rain gauges method MERGE2 (Novák, Kyznarová 2014; Novák, Kyznarová 2016) is run operationally to improve the rainfall estimates. The MERGE2 method generates the merged radar – rain gauge rainfall estimates (called MERGE product or simply MERGE). It also produces an adjustment coefficient that is further used to adjust radar-only rainfall estimates (for applications, including FFI, where there is a need for processing before merging with in-situ observations) and radar-only extrapolation (nowcasting) forecasts. The MERGE2 method was developed as a universal tool for all types of rainfall and it was not targeted at any specific hydrological model or application. All the calculations are based on moving 1-hour rainfall sums.

The adjustment coefficient, also called Mean Field Bias (MFB), is a robust conservative scalar coefficient computed as a ratio between the sum of 1-hour rainfalls measured by rain gauges over the territory of Czechia and the sum of corresponding 1-hour radar-only rainfall estimates (radar estimates at the grid points where the rain gauges are located). Rain gauge measurements are summed not only on the basis of the current (latest) time of observation, but previous measurements are also used. The time window used for the summation is dynamic (ranging between 3 hours and 3 days), depending on available rainfall data. The summation process is finished when a sufficiently large sum of

rain gauge measurements (currently 100 mm) is obtained. The weights of older rainfall measurements decrease exponentially.

The MERGE product is calculated using kriging with external drift (KED), where rain gauge measurements are interpolated and the radar field is used as an external drift field. KED is one of the best available geostatistical methods for calculation of combined radar – rain gauge rainfall estimates (Goudenhoofdt, Delobbe 2009) with application in various countries. The primary MERGE products are moving 1-hour sums of rainfall estimates, and their calculation is updated every 10 minutes. The MERGE method also generates other sums for longer time intervals (e.g., 3 h, 6 h, 12 h, 24 h). These sums are calculated as moving sums of the primary 1-hour products.

(a)

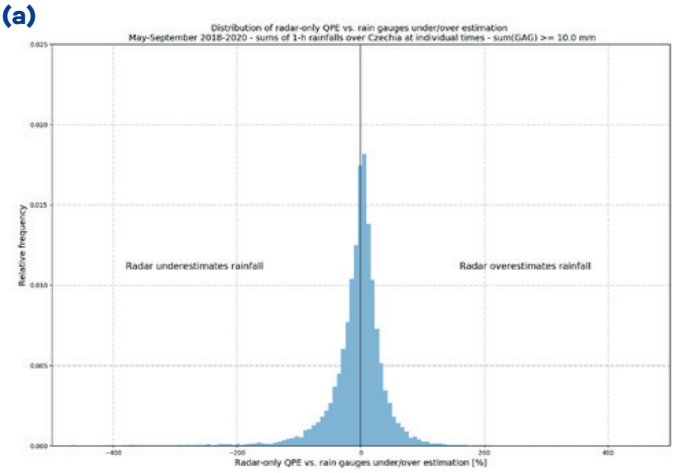

(b)

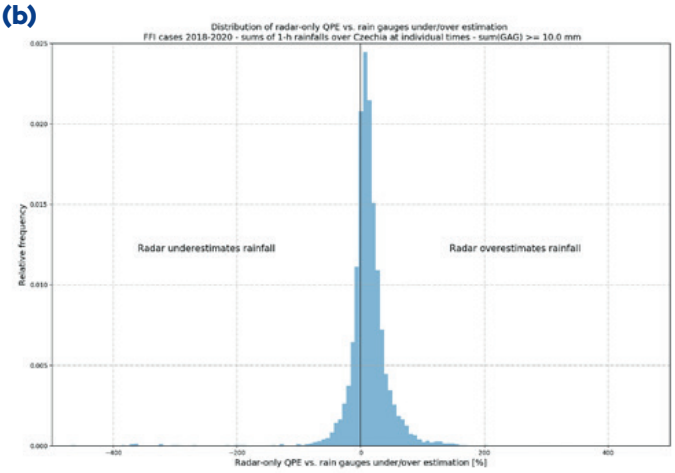

Fig. 6.1 Distribution of radar-only QPE vs. rain gauge under/over estimation. Comparison is based on sums of 1-hour rainfalls over Czechia. The distribution is calculated for estimates at individual times with 10-minute step during May–September 2018–2020 (a), and during selected significant FFI cases between 2018 and 2020 (b) when areal sum of rain gauge measurements over Czechia was ≥ 10.0 mm.

So called adjusted radar QPEs (the radar-only estimates multiplied by the adjustment coefficient) are typically worse than the MERGE estimates. The reason for applying the adjustment coefficient is that the adjusted radar QPEs can substitute the KED products in cases when the KED application is numerically impossible or the result would be problematic (too low correlation between radar and rain gauge values or not enough non-zero rain gauge measurements). The second reason is that the adjustment coefficient can be applied also to the radar-only estimates or forecasts when rain gauge measurements are not yet available to calculate MERGE (rain gauge measurements are available for the MERGE calculation process approx. 20 minutes after the nominal time). An example of such application is the provision of radar estimates just for the FFI. The FFI needs these data as early as possible. Delays associated with the MERGE product availability are not acceptable. That is why the last available adjustment coefficient is used to adjust the radar-only estimates and forecasts. These products, on

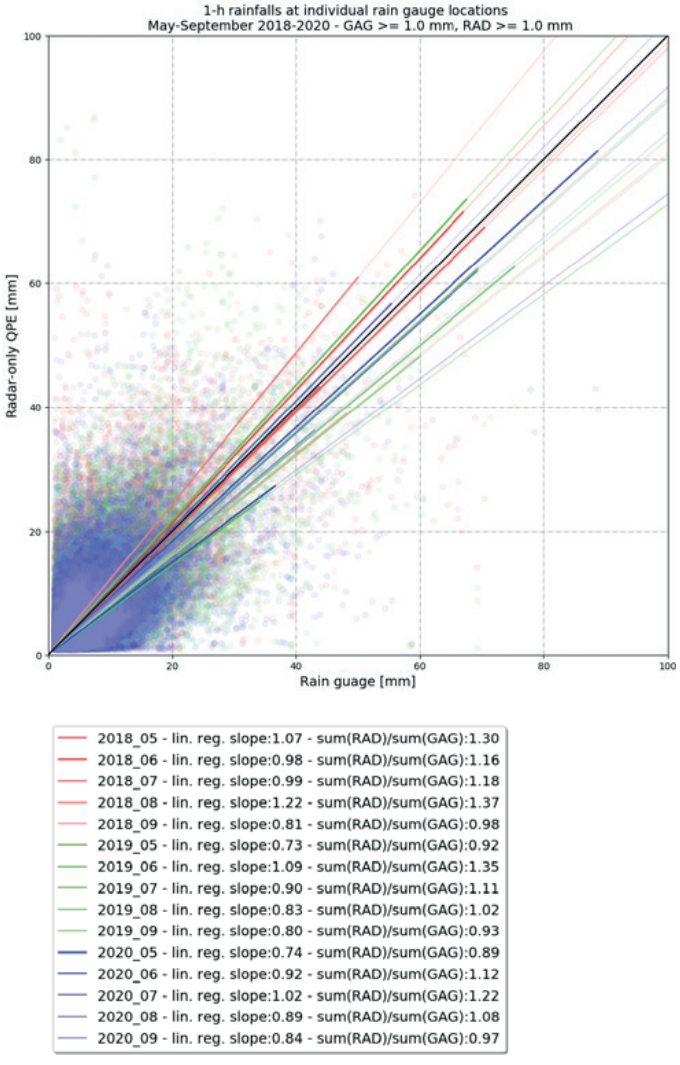

Fig. 6.2 Comparison of 1-hour rain gauge rainfalls and radar-only estimates at individual rain gauge locations during May–September 2018–2020.

the other hand, are available with the delay of 1 or 2 minutes after the nominal time.

Before upgrading the Czech weather radar network in 2015, the radar-only rainfall estimates typically underestimated the real rainfall intensity. There were also problems caused by unfiltered RLAN/Wi-Fi interferences and persistent ground clutters caused by the wind farms. New polarimetric weather radars were installed in 2015 (Novák 2016; Novák, Kyznarová 2016) and new dual-polarization measurements enabled much more effective filtering of such non-meteorological echoes. They also enabled the correction of radar signal attenuation in strong precipitation, which, together with improved radar calibration, led to a decrease in bias of the radar-only rainfall estimates. As shown in Fig. 6.1 (a) and Fig. 6.2, the radar-only rainfall estimates are currently not biased, which means that radars are correctly calibrated and the coefficients of the Marshall-Palmer equation are correctly chosen. Figures also show the variability of radar rainfall under/over estimation, in comparison to the rain gauge measurements, which are caused by the natural variability of drop size distribution in the precipitation clouds, but also by other factors, e.g., evaporation of precipitation in the lower parts of the atmosphere before reaching the ground, or the issue of comparing point rain-gauge measurements with the mean areal radar estimate over the grid area 1×1 km, which often do not correspond, especially in convective rainfall that is often highly variable. While radar-only rainfall estimates are not biased if we evaluate the whole warm seasons 2018–2020, the slight overestimation is apparent when only significant FFI cases with intense convective rainfall (see Chapter 6.1.3 for details) are evaluated, as depicted in Fig. 6.1 (b).

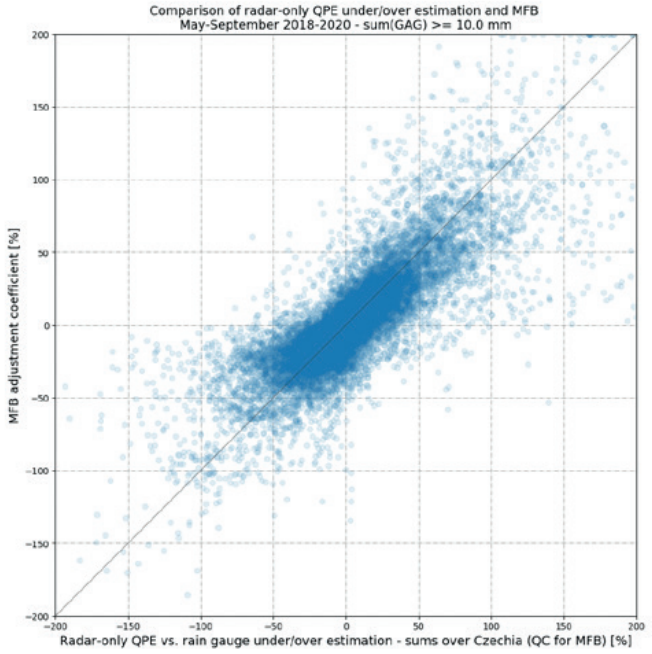

Fig. 6.3 Comparison of under/over estimation of the areal sum of the radar-only 1-hour rainfall estimates and the MFB adjustment coefficient during May–September 2018–2020.

Comparison of individual radar-based rainfall estimates (Novák, Kyznarová 2014; Novák, Kyznarová 2016) showed that the adjusted radar QPEs improve the radar-only estimates. Improvement is more significant in cases of systematic under/over estimation of radar-only rainfalls (typical of previous generation of radars operated until 2015). As can be seen in Fig. 6.3, the adjustment coefficient is not biased but it is scattered. This scatter is caused by the con-

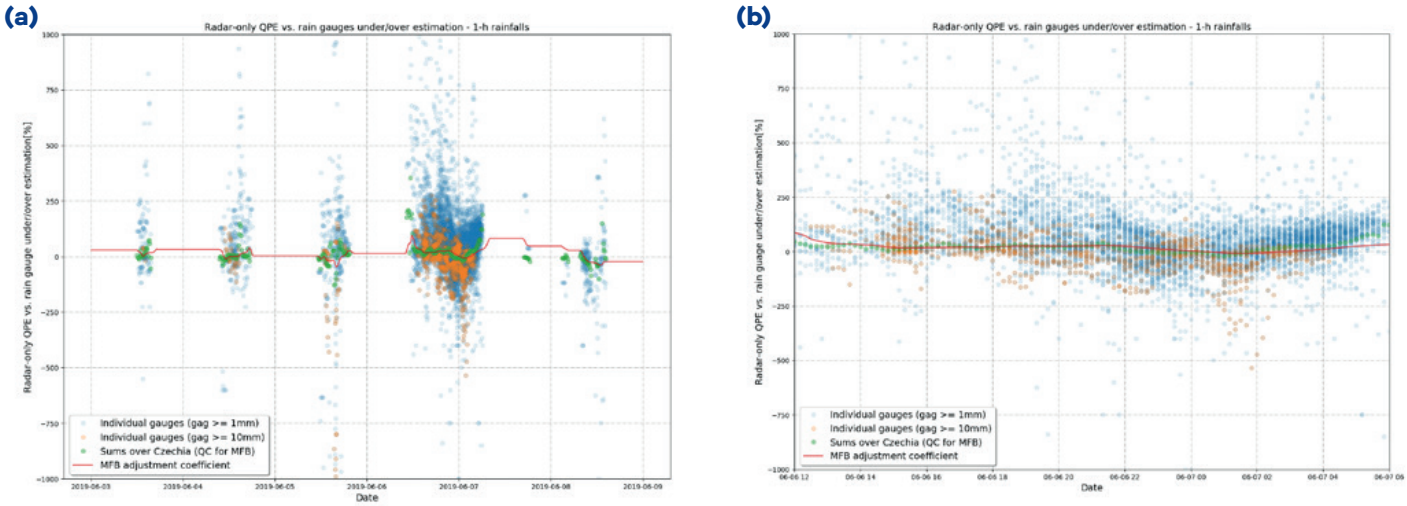

Fig. 6.4 Example of radar under/over estimation variability for 6 days from June 3, 2019 to June 9, 2019 (a), and a detailed view of variability over 18-hour period from June 6, 2019 12:00 UTC to June 7, 2019 06:00 UTC (b). Examples depict one of the episodes with selected significant FFI cases of intense convective rainfall (as explained in Chapter 6.1.3). Intense rainfalls with FFI response were identified from June 4, 2019 to June 6, 2019.

servativeness and robustness of the scalar adjustment coefficient averaged over whole Czechia and the time window. This is exactly why in some cases the adjusted radar QPEs are not corrected enough. In those cases, the radar-only rainfall estimates significantly overestimated real rainfall. The adjusted radar QPEs decreased this overestimation but not enough, and such remaining overestimation caused problems to the FFI operation, as demonstrated in the next chapter.

The adjustment coefficient does not fully correct the radar-only rainfall estimates in some cases because of the spatial and temporal variability of rainfall and its physical parameters, leading to the variability of the radar-rain gauges ratio. In some cases, the ratio between radar and rain gauge measurements may vary in different parts of Czechia. Therefore, a spatially variable adjustment coefficient was also used in the past. However, such adjustment coefficient did not yield good results when applied to the extrapolated radar-only rainfall forecasts. The problem with the spatially variable adjustment coefficient lies in different physical nature of the effects that cause radar rainfall under/over estimation; some are stationary over time (e.g., orography shielding, partial bright-band detection, evaporation of precipitation in dry low levels of the atmosphere), and some are variable and relate to particular precipitation clouds (e.g., specific drop size distribution in clouds). When the adjustment coefficient is applied to the radar extrapolation forecasts (up to 3 hours ahead), it is not possible to determine how various effects influence different parts of the domain and, thus, it is not clear how the adjustment coefficient should be applied (should it be stationary, or should it be changed based on radar derived wind field?).

There is also an issue with big temporal variability of the radar-rain gauge ratio. The use of moving time window for the calculation of the adjustment coefficient is intentional in order to smooth this big variability, which, otherwise, could cause overcorrection mainly in cases when the coefficient is applied to the extrapolation forecasts. On the other hand, there is some time delay needed to accommodate the adjustment coefficient to temporal changes of the radar-rain gauges ratio.

The variability of radar under/over estimation (radar-rain gauge ratio) is graphically demonstrated in Fig. 6.4.

Even though the adjustment coefficient improves the radar rainfall estimates, the best areal radar-based rainfall estimates are obtained through the MERGE product that should be used every time it is possible.

So far, the use of MERGE has only been possible in a daily step (24-hour sums) because the basic moving 1-hour MERGE step is too long for the FFI purposes, for which the shortest time interval (10–15 minutes) must be used. The second reason is the non-homogeneity of the MERGE data and the adjusted radar QPEs, as the adjusted radar QPEs tend to be significantly overestimated compared to the amounts of MERGE precipitation.

6.1.2 Input data quality and reliability

When computing the soil saturation, 24-hour rainfall totals and actual evapotranspiration are needed. In fact, evapotranspiration is estimated using a model fed by other variables (proxies) measured at climatological stations (Kohut et al. 2011). Therefore, the quality and reliability of such data depend on the employed model and the input values of the other variables. If evapotranspiration values at a station appear to be suspicious in a comparison to other stations, such a station may be removed from the computation.

For the derivation of the areal 24-hour rainfall totals, the MERGE product is utilized.

Estimation of the current flash flood risk makes use of rainfall estimates from the adjusted radar QPEs in a time step of 15 minutes.

In 2014, the QPE methodology was changed regarding the computation of the adjustment coefficient, as well as the MERGE method. In addition, as already mentioned in the previous chapter 6.1.1, both meteorological radars were replaced in autumn 2015. This led to a substantial change in input data for FFI, see Figs. 6.5 and 6.6.

Figures 6.5 and 6.6 show the 24-hour sum from the radar-only data (top-left panel) and the 24-hour sum from the adjusted radar QPEs (top-right panel). The bottom panel represents the final product of the MERGE method.

Figure 6.5 displays the situation before the change of the computation methodology and the meteorological radars replacement. Specifically, the 24-hour rainfall totals on May 28, 2014 06:00 UTC are depicted in Fig. 6.5. It was characteristic of this period that the raw-radar rainfall estimates were underestimated in comparison to real rainfall totals. The adjustment coefficient was treated as spatially variable. Apparent beams can be seen in the figure, caused by the radar signal interference with the signal of Wi-Fi transmitters.

Figure 6.6 represents the 24-hour sum of rainfall estimates on June 16, 2019 06:00 UTC. It shows the situation after the meteorological radars replacement and the change of the computation methodology adjusting radar data, and the derivation of the MERGE product. Here, on the other hand, the overestimation of rainfall by radar-only data can be seen when it comes to the comparison with real rainfall totals. In the new method of adjusted radar QPE product derivation, the variable magnitude is preserved regarding the time, but

only one value of the coefficient is calculated for the whole territory of Czechia. Its starting value is set to 1.0. Among other aspects, this leads to overestimation of the adjusted radar QPEs values in comparison to those measured at rain gauges, which is particularly typical for initial stages of rainfall events. Based on the analysis performed in 2018–2020, it was found that rainfall totals greater than 10 mm·day^{-1} have been, on average, overestimated by about 10% by the adjusted radar QPEs, see more in Chapter 6.1.3.

The fact that, apart from some exceptions, the radar signal interference with the signal of Wi-Fi transmitters was eliminated may be considered positive. False reflections, e.g., from ground targets, were also reduced; they, however, may still be manifested in the data from time to time, e.g., from wind power plants located in the Ore Mountains. This problem is, in fact, not spatially extensive, and it has been satisfactorily eliminated through advanced

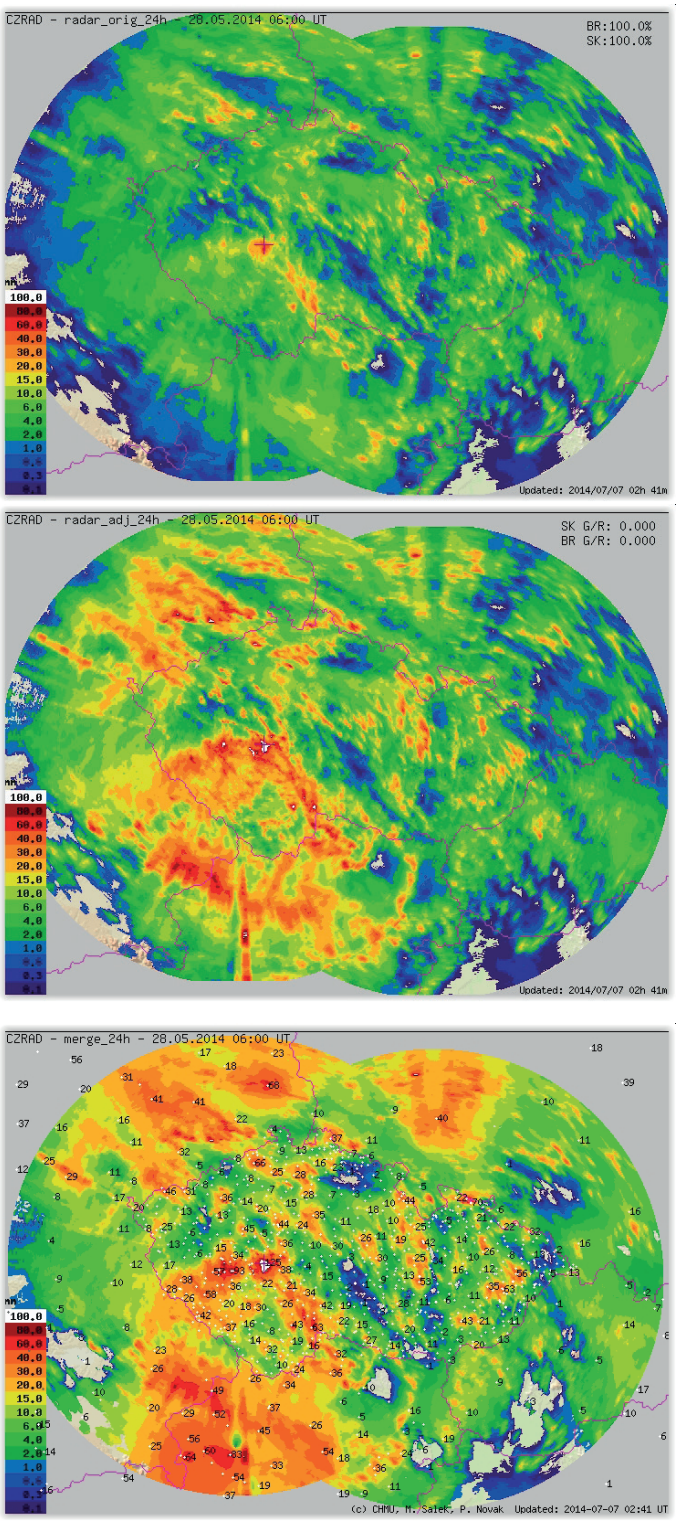

Fig. 6.5 Sum of 24-hour radar-only QPE (top), adjusted radar QPE (middle), and MERGE QPE (bottom) on May 28, 2014 06:00 UTC.

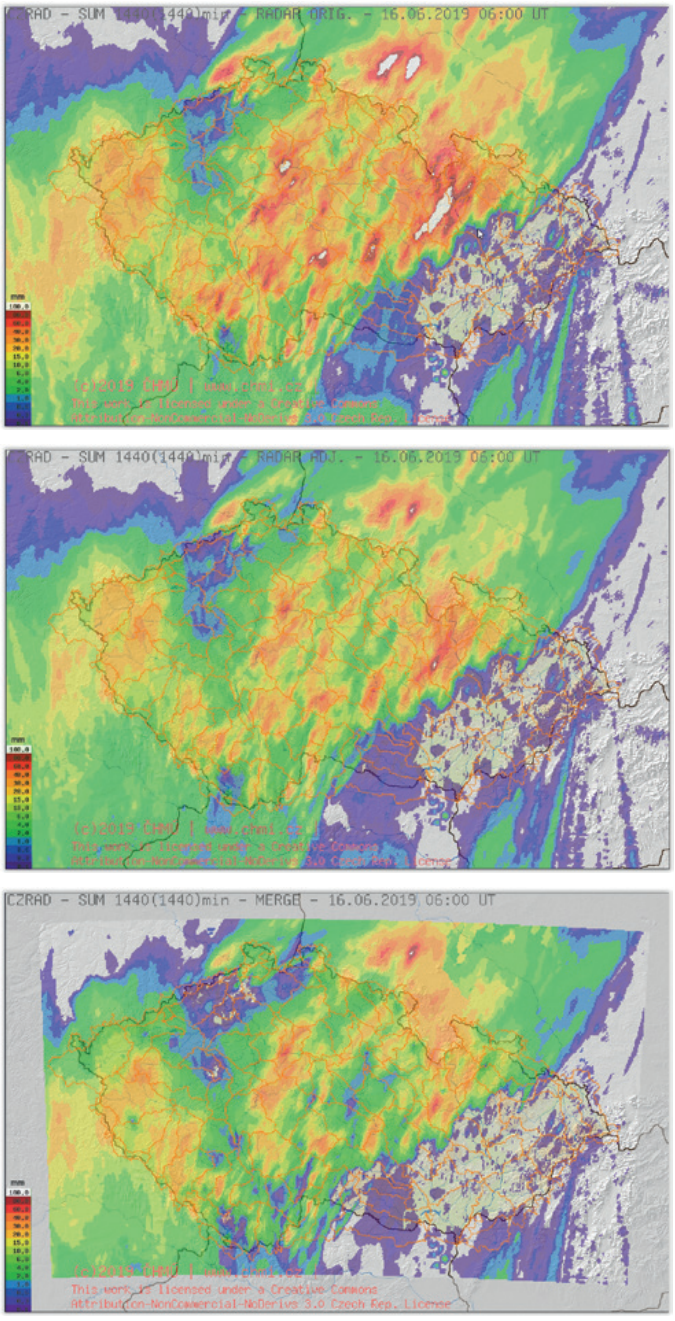

Fig. 6.6 Sum of 24-hour radar-only QPE (top), adjusted radar QPE (middle), and MERGE QPE (bottom) on June 16, 2019 06:00 UTC.

signal processing of modern polarimetric radars in recent years.

The overestimation due to use of adjusted radar QPEs led to many false alarms in the FFI. Thus, after the convective season 2016, the threshold values in the FFI computation routines had to be modified/re-evaluated for the period 2017–2020, see more in Chapter 6.4.

QPE overestimation is not limited to convective events, but may be present even in cases of spatially extensive stratiform precipitation, when the height of the zero isotherm decreases towards the altitude of 2 km above mean sea level and the bright-band contaminates the radar reflectivity product used for QPE, see Fig. 6.7. If the soil is significantly saturated, this fact might results in flash flood risk false alarms.

The MERGE product is a combination of radar rainfall estimates and ground measurements at rain gauges. Therefore, besides possible errors in radar measurements, it is necessary to check for the errors in the measurements of automatic rain gauges. The errors in such measurements might be quite easily detectable by human eye tracking (comparing the images of the radar-only, eventually adjusted radar), but almost impossible to be successfully revealed by automatic algorithms.

In Fig. 6.8, the circle represents an apparent error in measurement, which was likely caused by a jammed rain gauge. The left panel displays the 24-hour sums from the adjusted radar QPEs, while the right panel shows the final MERGE product. It is clear from the adjusted radar QPEs that there were rainfalls at the site of the rain gauge, even though the rain gauge itself measured no rainfall.

If the rain gauge is jammed, the water may flow through it later (possibly next day), and MERGE can show a value at the site of the rain gauge that does not correspond to the radar data.

Therefore, 24-hour sums of the radar estimates and those of MERGE should be human-checked and the suspicious values of the 24-hour sums of radar estimates should be

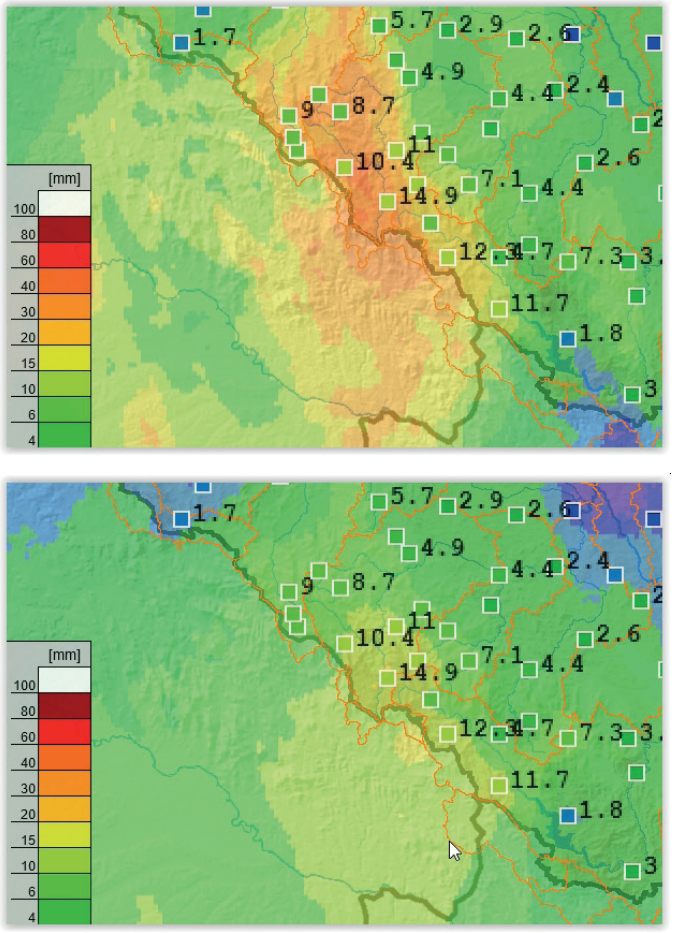

Fig. 6.7 Sum of 3-hour adjusted radar QPE (top) and MERGE QPE (bottom) on August 4, 2020 10:00 UTC. Point symbols represent locations of climatological and precipitation stations and the respective numbers are the precipitation totals over a certain period.

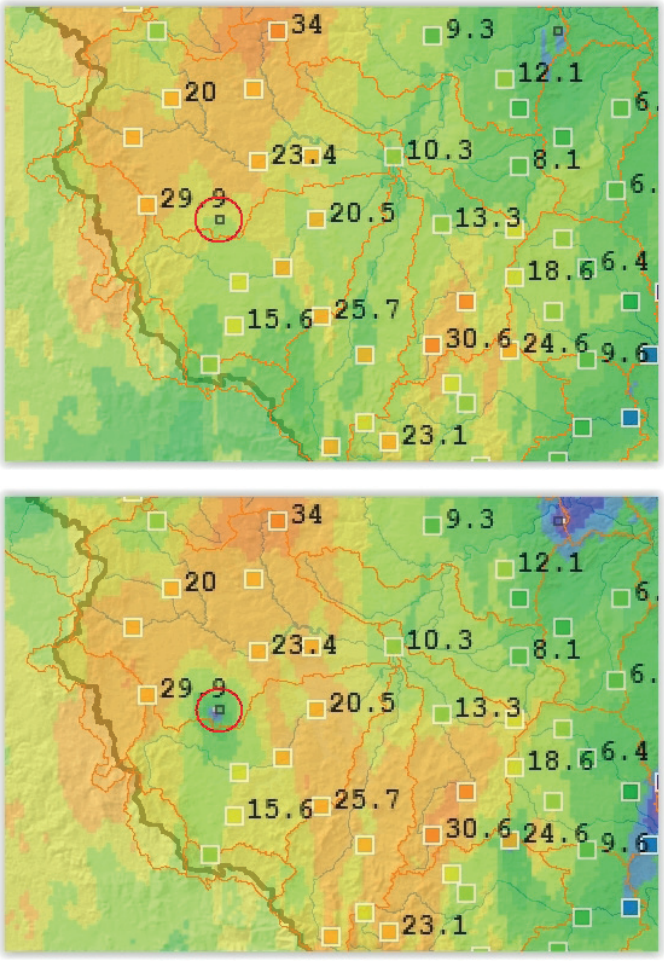

Fig. 6.8 Sum of 24-hour adjusted radar QPE (top) and MERGE QPE (bottom) on June 16, 2019 06:00 UTC. The circle indicates a possibly incorrect rain gauge measurement.

eliminated when computing the saturation indicator. At the CHMI, the procedures were put into practice that allow the suspicious values in the database to be manually flagged (grey-listed), which, in turn, does not allow such rain gauge data to enter the MERGE computation.

Tab. 6.1 Overview of selected rainfall events in 2018, 2019 and 2020 (FFI cases).

Year	Number of selected events	Count of paired values	Mean rain gauge measured rainfall total [mm]	Mean adjusted radar QPE total [mm]	Geometric mean of ratios
2018	16	888	22.4	26.0	1.13
2019	17	1267	20.9	21.8	1.02
2020	22	1842	20.6	22.4	1.07

Detection of rain gauges that measure inaccurately from a long-term point of view is more difficult. Such detection is only possible by comparing the measurements in the neighbourhood during a considerably longer period (e.g., by comparing monthly precipitation totals). Inaccurately measuring rain gauges are black-listed and no longer enter the computations.

6.1.3 The analysis of adjusted radar QPEs as an input to the FFI

The main purpose of this analysis was to compare the 24-hour sum of adjusted radar QPEs provided for the FFI against the 24-hour precipitation totals measured at rain gauges for selected rainfall events in 2018, 2019 and 2020.

While the performance of the MERGE product in the FFI is satisfying (only optimization of the manual check of rain gauges is discussed), adjusted radar QPEs tend to overestimate the precipitation significant for the FFI, which consequently leads to FFI false alarms. To analyse the problem in more detail, the cases with the flash flood occurrence or flash flood risk indicated by the FFI were identified in all the periods May–September 2018–2020. Every case was represented by 24-hour interval from 06:00 to 06:00 UTC. These cases were further called the 'FFI cases'. The FFI cases were defined by the following criteria:

– 24-hour rainfall totals reached or exceeded 10 mm in at least 10 rain gauges during particular rain event,

– the precipitation was exclusively convective,

– the events with stratiform precipitation, even orographically amplified, were not considered,

– the FFI detected the risk of a flash flood or local flooding occurrence, or there was direct evidence of a flash flood occurrence.

Since adjusted radar QPEs are the main precipitation input into FFI rainfall-runoff modelling, it is very important to know the ratio between QPEs and observed precipitation, indicating whether QPEs are overestimated or underestimated in average for events with flash flood or local flooding potential.

The measured 24-hour rainfall and corresponding radar QPE values at rain gauge locations derived from the grid with the 1 km^2 cell size were paired together and evaluated. Evaluation showed that, during the FFI cases, the adjusted radar QPE, on average, overestimated significant rain gauge measurements by about 10%, as summarized in Table 6.1. It was further shown that, in the FFI cases, radar-only QPEs also, on average, overestimated rain gauge measurements, as depicted in Fig. 6.1 (b). During the FFI cases, the overestimation of radar-only QPEs was higher than that of adjusted radar QPEs. Thus, the adjustment coefficient seemingly corrects the radar-only estimates, but not enough.

The overestimation of adjusted radar QPEs versus actually measured values at rain gauges for convective events had to be taken into account by adjusting the parameters of the FFI calculations.

As the overestimation of the input data can be considered a serious problem, the further development of FFI was therefore focused on changing the way of adjusting the radar data (Novák et al. 2021) and the possibility of using the MERGE product even for shorter time intervals. More information is given in Chapter 6.5.

6.2 Influence of initial conditions setup

Setting up the initial conditions is very important for the correct functionality of the FFI. Its impacts are, of course, the greatest in the first few weeks of a warm-up period after the initialization of the FFI for a given season. After some time, the effect weakens, but it may still play an important role.

Because the FFI is not equipped with a component accounting for snow accumulation and melt, the day of activation is selected from those when the snow cover occurs only in

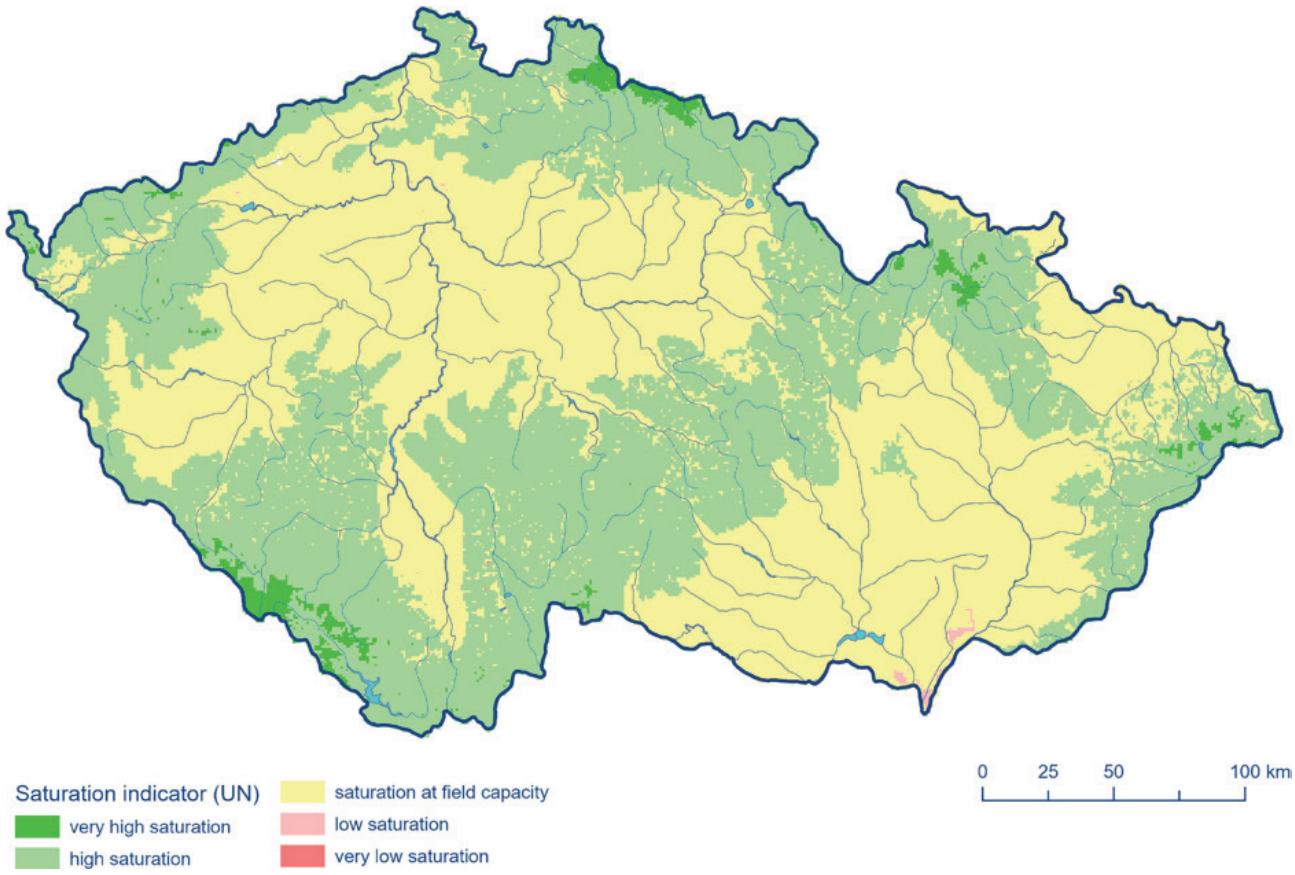

Fig. 6.9 Soil saturation indicator values valid for April 12, 2020 06:00 UTC.

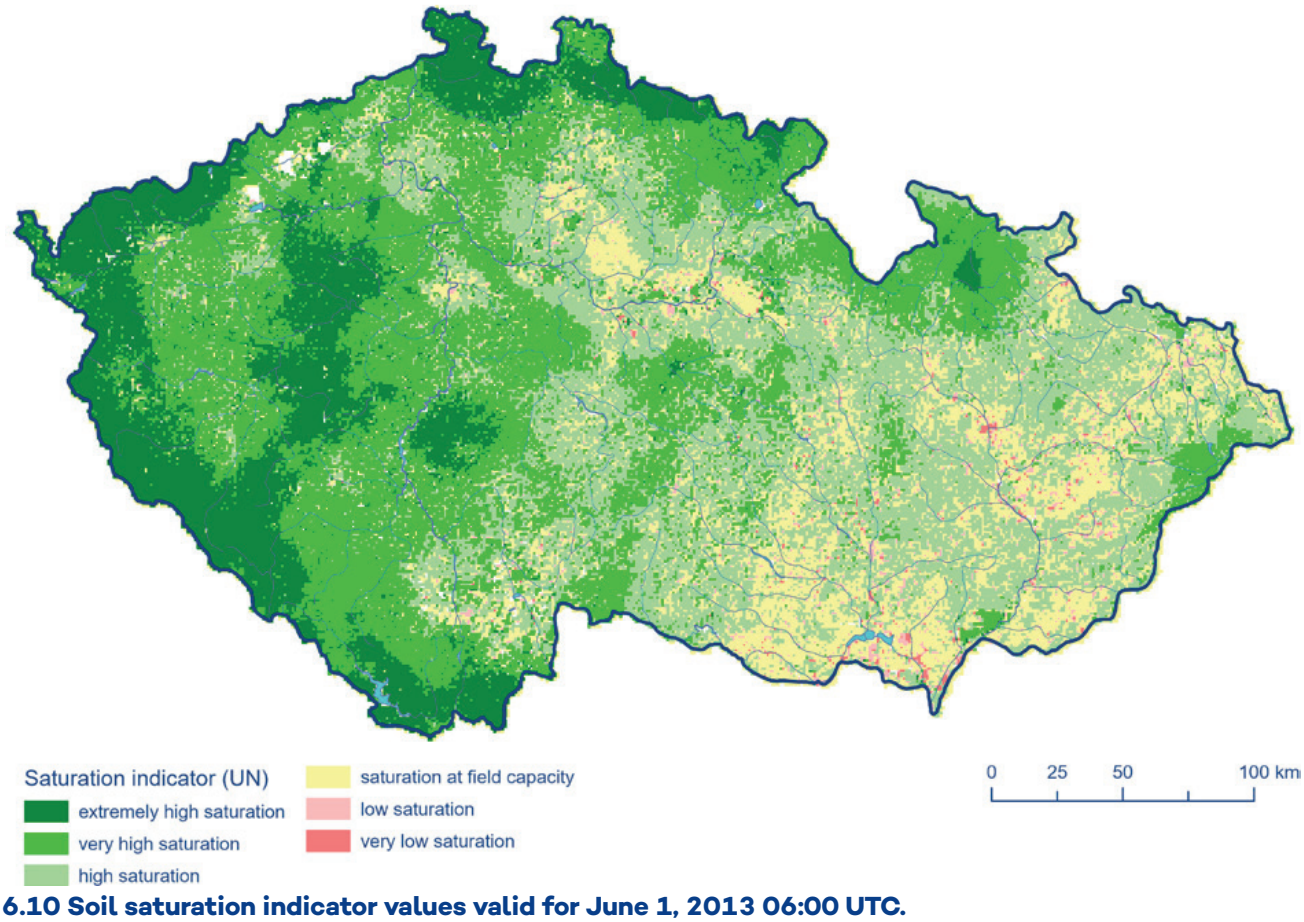

Fig. 6.10 Soil saturation indicator values valid for June 1, 2013 06:00 UTC.

the highest mountain ranges, which happens in Czechia typically in the first half of April. For the setup of the initial conditions, it is necessary to assess the current saturation of the top layer of soil over the whole territory of Czechia. In particular, the data from the CHMI climatological stations are taken into consideration where soil moisture is measured at various depths. Furthermore, one can employ the maps of modelled soil moisture, which are regularly produced by competent CHMI climate department experts. If the mountainous areas are still covered with snow, it is assumed that it will start to melt in several next days, which is reflected in setting up the initial conditions. In addition, comparison is carried out between flow rates in watercourses and their long-term monthly averages.

According to the above-mentioned information, the territory of Czechia is divided into a number of regions (ca 4–5) to which different *CN* values are assigned. In regions where high saturation is assumed, the values are usually close to CN_{III}, while in regions without previous winter snow cover and with below-normal soil moisture, the initial values of saturation can even be below the CN_{II} value.

Values of the current soil saturation are further updated based on daily re-calculations. In the future, satellite products can be used as well, these can offer qualitatively different data of soil saturation estimates at least at the top layer of soil. By comparing the outputs of satellite data with the FFI calculations, regular verification of the values of the current soil saturation might be possible.

In Fig. 6.9, the estimate of initial conditions on April 12, 2020 can be seen. The snow cover occurred only in high mountain ridges. This estimate was based on the fact that the previous winter season was characterized by small or complete lack of snow cover, while the snow cover virtually did not occur in low and mid-altitudes, and it was below average even in the mountain areas. At the same time, the winter season was above normal regarding temperature, while it was below normal in terms of precipitation, except for February. In the middle of April, river discharges ranged between 20 and 40% of average April values. Therefore, the *CN* values set for lowlands were estimated to be around CN_{II}. Only for the highest mountain areas, the values were set to CN_{III}.

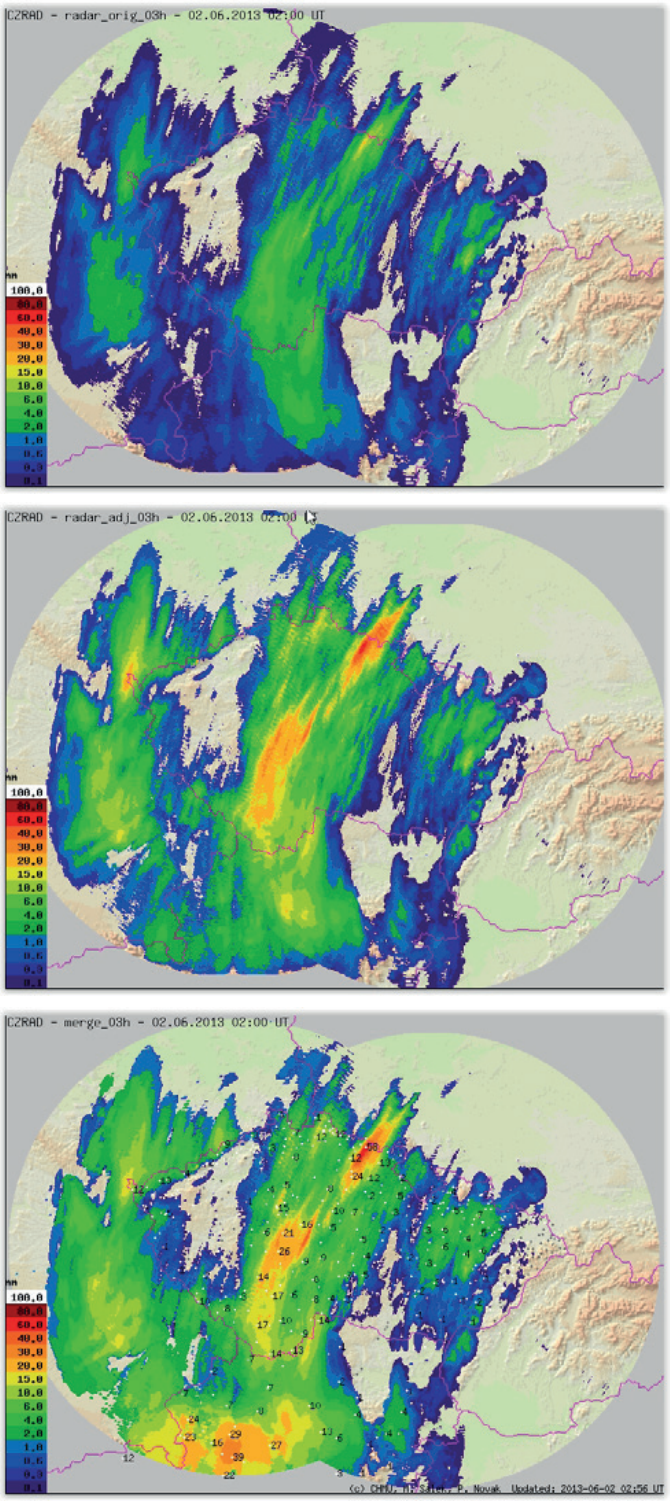

Fig. 6.11 Sum of 3-hour radar-only QPE (top), adjusted radar QPE (middle) and MERGE QPE (bottom) on June 2, 2013 02:00 UTC.

6.3 Assessment of FFI performance during the June 2013 flood

At the beginning of June 2013, a significant rainfall-runoff event occurred that affected western parts of the Czech Republic. During this situation, torrential rainfalls were combined with intense continuous rainfall resulting in widespread flooding of streams and rivers. In addition, catchments were highly saturated before the event due to significantly wet May, see Fig. 6.10.

Rainfall lasted from the afternoon hours of June 1, 2013 to the afternoon hours of June 2, 2013. Figure 6.11 shows the

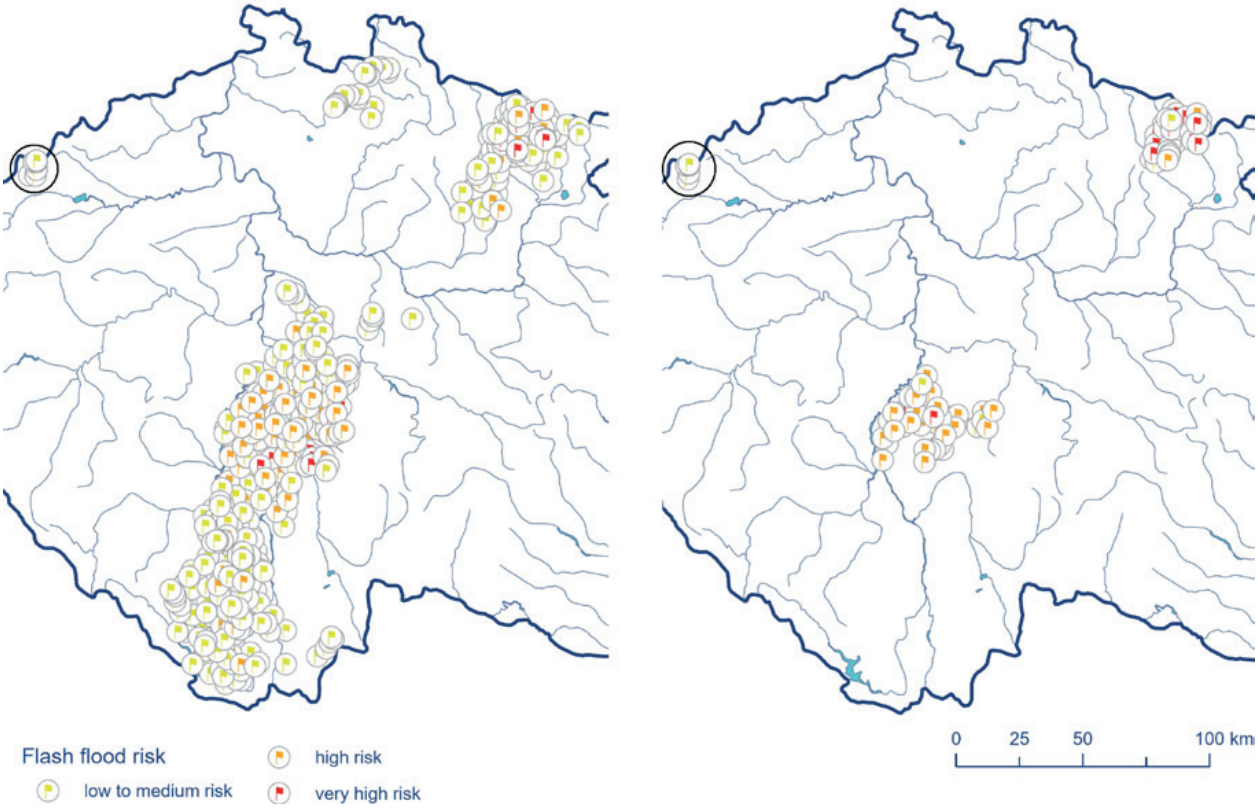

Fig. 6.12 Flash flood risk assessed in individual catchment areas on June 2, 2013 02:00 UTC. The large circle indicates the designated area where the wind farms are in operation.

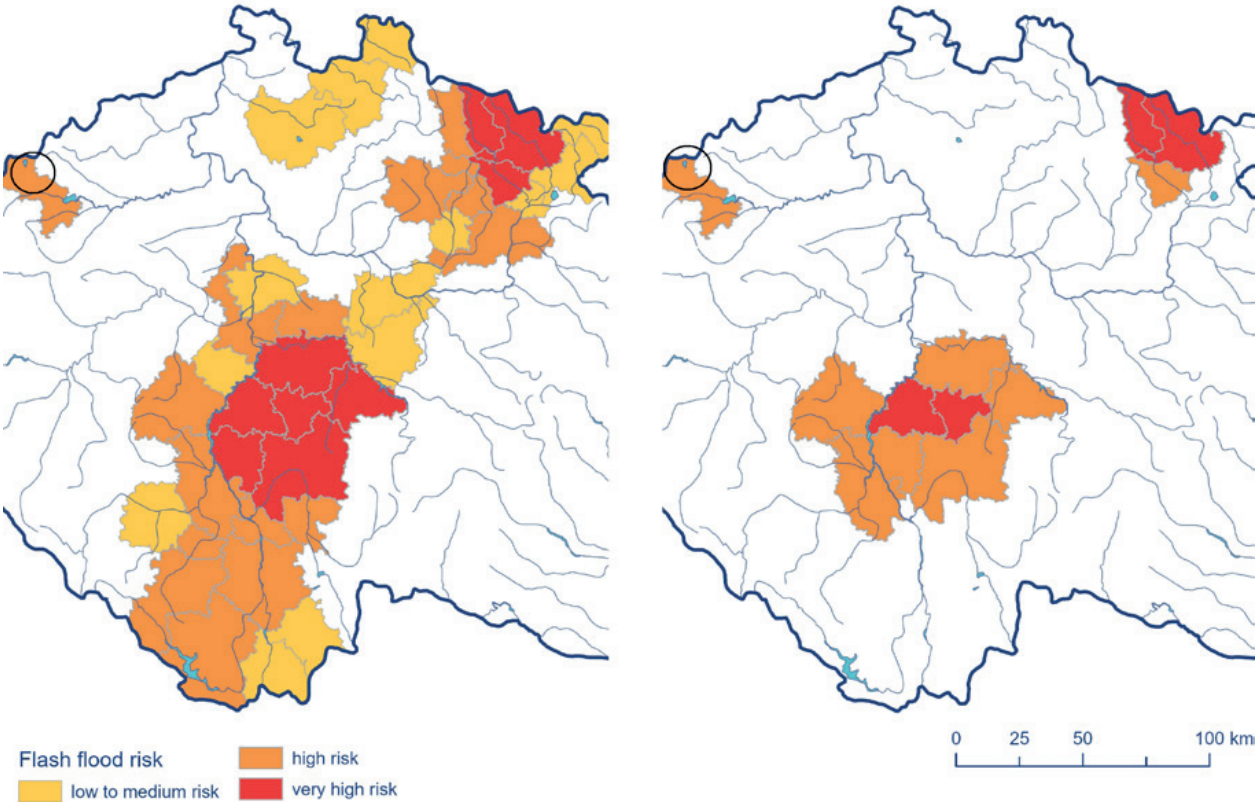

Fig. 6.13 Flash flood risk assessed for individual districts on June 2, 2013 02:00 UTC. The circle indicates the designated area where the wind farms are in operation.

3-hour sum of rainfall for the period from 23:00 to 02:00 UTC. The top-left panel represents the radar-only rainfall estimates, the top-right panel displays the adjusted radar QPEs, and the bottom panel depicts MERGE QPE. It is apparent that the radar-only QPE was considerably underestimated. In this time period, local torrential rainfalls occurred together with intense stratiform rainfalls combined with a substantial convective and wind shear component.

Large area hit by rainfall combined with strong previous soil saturation resulted in a large number of catchments for which the flash flood risk was calculated. The FFI calculations took tens of minutes (exceeding time slot before new rainfall data inputs delivery), which led to the need for setting up a limit of the number of catchments for which the computation was conducted to ensure that calculations were done in time. Since that situation, the FFI performs the selection of catchments with the highest ratio of the calculated Extremity Index to the IE_{100} value.

For comparison, re-simulation of the FFI calculations was carried out. The results are documented in Fig. 6.12 and Fig. 6.13. The left panel shows the results for the run in which the number of catchments was not restricted. The right panel depicts the situation in which the selection was performed.

Fig. 6.13 proves that, when limiting the number of catchments, the flash flood risk was not detected at all for some MEPs, eventually a lower flash flood risk was calculated. This is determined by the fact that the flash flood risk is calculated in the system of catchments, where the level of risk can rise downstream, which the selection procedure doesn't account for.

In Fig. 6.12 and Fig. 6.13, the circle highlights the area where the wind power plants were operating. Meteorological radar saw them as false targets, and specifically during the situation in June 2013, it resulted in the detection of the flash flood risk. After the replacement of the meteorological radars, these targets have been partially eliminated.

It must be noted that any similar extreme event (in the meaning of extent of affected area and total precipitation volume) was not observed in the territory of Czechia from June 2013 until the time of writing this report.

6.4 Evaluation of the period 2017–2020

In the framework of a research project (Borovička et al. 2020), detailed assessment was carried out of the FFI operation during years 2017–2019. At the end of 2020, a similar assessment was made for the 2020 convective season. Tables 6.4 and 6.5 summarize all the calculations of the risk within the FFI application for the period 2017–2020 for MEPs.

The least risk-inducing convective situations occurred in 2017 for both the flash flood risk (FF) and the risk of local

Tab. 6.4 Flash flood risk and local flooding in MEPs in the period 2017–2020.

Year	Type of risk	Days total with risk occurrence	FFI runs with risk detection	Risk level 1 total	Risk level 2 total	Risk level 3 total	Risk events total
2017	FF	22	171	320	88	4	412
	LF	36	186	429	73	29	531
2018	FF	33	398	589	326	114	1029
	LF	53	514	1036	294	277	1607
2019	FF	34	379	774	285	49	1108
	LF	41	364	906	183	91	1180
2020	FF	56	799	2299	911	253	3463
	LF	65	778	2080	668	645	3393

Tab. 6.5 General risk of flash flood occurrence in MEPs in the period 2017–2020.

Year	Days total with risk occurrence	FFI runs with risk detection	Risk level 1 total	Risk level 2 total	Risk level 3 total	Risk events total
2017	37	255	723	70	0	793
2018	53	626	1686	400	57	2143
2019	45	510	1672	178	35	1885
2020	68	1026	4402	888	156	5446

flooding (LF). In that year no general risk of the very high risk level 3 was recorded either, see Tab. 6.5.

During the years 2018 and 2019, risk warnings were more frequent, as a result of more frequent occurrence of convective situations, which also led to the substantial runoff from catchments.

The largest number of cases exceeding the risk threshold took place in the 2020 summer season. As early as during the spring months, rainfall was frequent, both convective and stratiform, and in combination with high soil saturation in some regions and many significant rainfall events led also to significant runoff events.

The assessment for the period 2017–2020 proved that calibration of the calculation parameters based on assessment of previous period enhanced overall performance of the system by reducing false alarms from radar QPE overestimation in 2015 and 2016. A number of alarms caused by the radar inference with reflections of other than meteorological origins decreased as well.

However, it must be understood that the assessment of the proportion of false alarms can hardly be precise and fully objective. The evaluation deals with difficulties regarding determination of 'reality'. Small catchments affected by the flash floods are mostly without gauging. Supporting information is provided by reports on interventions of rescue system in the affected locality at a given time, or from publicly available pictures and videos from random witnesses of the flood event. If torrential rainfall hits an uninhabited area, where there is no hydrological observation, the evaluation of the FFI application procedures performance is even more difficult. So uncertainty in the evaluation is likely to remain. Currently, however, procedures are set to capture all very significant flash floods, in case of less significant flash floods certain number of undetected flash floods is anticipated. There was virtually no significant flash floods in the assessment period for which the FFI did not calculate at least a level 2 or 3 risk.

It can be concluded that the FFI was operating reliably during most significant rainfall-runoff events in the 2018–2020 period, but there is still work to be done to remove false alarms that are caused by the overestimation of the adjusted radar QPEs (whether in regional stratiform or local torrential rainfall) over the territory strongly saturated from previous precipitation.

6.5 FFI development

Reliable input data are fundamental for successful operation of the FFI application. Therefore, adjustment method aimed at radar data is considered to remain key future area of development. At the same time, regular operational and careful data quality control of rain gauges has to be ensured.

As part of the research project "Hydrometeorological risks in the Czech Republic – changes and prediction enhancements" implemented since 2019, a new method of adjusting radar data has been developed. A new adjustment coefficient has been designed specifically for the FFI focusing on flash floods nowcasting. The focus has concentrated on prioritizing intense rainfalls, decreasing the averaging time window and development of a spatially variable adjustment coefficient.

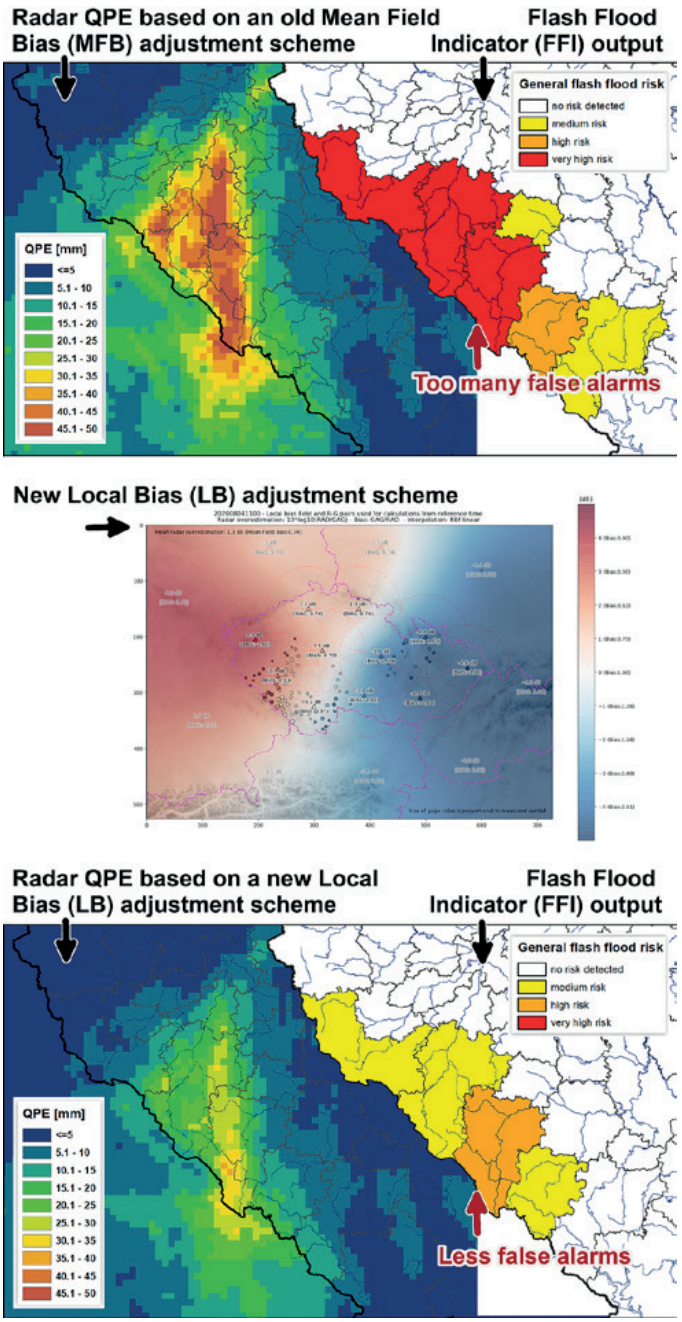

Fig. 6.14 Comparison of FFI outputs according to old (MFB) and new radar data adjustment (LB).

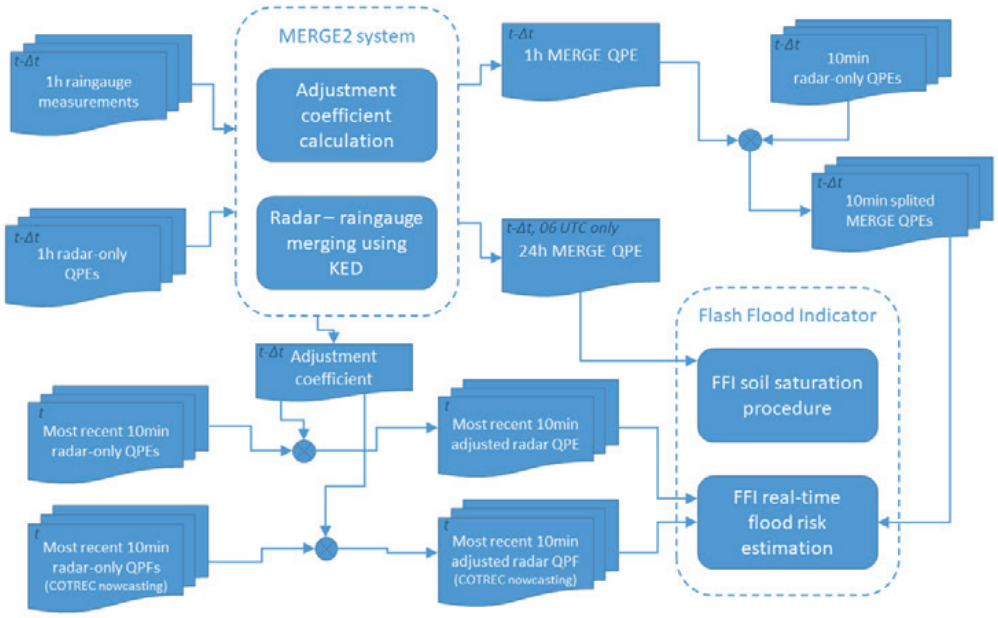

Fig. 6.15 Diagram of the radar-based QPE/QPF processing as an input data into FFI.

A diagram of the radar-based QPE and QPF processing as an input into FFI is shown in Fig. 6.15. This figure describes MERGE2 method and radar QPE/QPF adjustment as described in Chapters 6.1.1 and 6.1.2 and also MERGE QPE splitting.

As already mentioned, the set-up of initial conditions is very important, regarding mainly the soil saturation, which significantly influences the further development of the saturation values during the year. Thus, from a viewpoint of better reliability of the detection of the flash flood risk, it is suitable to choose the initial conditions concerning the saturation state based on a thorough analysis of soil moisture measurements. In the future, the utilization of satellite products is planned for the evaluation of the initial soil saturation during April, when the FFI is usually activated. If the satellite imagery proves to be usable, the verification of the saturation during the year may eventually be also enabled.

The new method of adjusting radar data based on Local Bias (LB) is described in the report by Novák et al. (2021) where the adjustments have been tested on four episodes which occurred in 2020. The results are promising in the sense that there could be a significant reduction in false alarms in cases of heavy stratiform precipitation in the conditions of high soil saturation (see Fig. 6.14).

Another quality improvement of the radar QPE input into the FFI will be achieved by splitting the 1-hour MERGE product into shorter 10-minute sums. When dividing 1-hour sums of the MERGE into 10-minute intervals, corresponding 10-minute radar-only sums are used in each interval as specific weights.

These divided 10-minute MERGE intervals should be even more accurate than adjustment fields, but they are not available for approx. the last half an hour and for the nowcasting[6]. For this time span, the adjusted radar QPE based on the new adjustment method (LB) will be used.

Radar QPEs based on the new adjustment method as well as on the divided 1-hour MERGE product enter the FFI calculations from the convective season 2022. As these new QPEs are qualitatively and quantitatively new input data, qualitatively different outputs regarding the flood risk estimation can also be expected. These outputs will need to be closely monitored and after their evaluation, and recalibration of some FFI parameters, can be applied.

With respect to relative time-consuming calculations performed by the FFI, it is necessary to operate the FFI application on a powerful server, which may further shorten the interval of computation as well.

Public outreach is equally important to ensure the effective use of the system by the end-users. While basic information about FFI and benefits it brings are presented at webpage of the CHMI or through social networks, further efforts need to be invested in direct access to and feedbacks from priority user group of local administrations.

6 The implemented nowcasting method performs only trajectory extrapolation of already existing thunderstorm cells, therefore it cannot capture their development.


UHELNÁ

7. Conclusion

The main task of the FFI (Flash Flood Indicator) system is to detect the potential flash flood risk. The system was developed between 2008 and 2011 and was put into testing in June 2010.

The system consists of the following main components:

– calculation of the current soil moisture conditions over an area in a daily step based on the water balance of rainfall, runoff and actual evapotranspiration,

– calculation of potentially dangerous amounts of rainfall of durations of 1, 3 and 6 hours, which may cause significant surface runoff,

– an estimate of the general flash flood risk based on 10-minute radar rainfall estimates (including nowcasting) and defined runoff thresholds. The general flash flood risk is computed as a combination of the local flooding risk and the flash flood risk by using the schematic of hydrologically connected river basins and reaches.

Individual procedures can be run either interactively (using the GIS environment) or as scheduled tasks.

Outputs from procedures of calculation of actual soil moisture conditions, potential rainfall estimates and the flash flood risk are presented in several ways:

– on the CHMI website,

– through the web map application 'Flash Flood Indicator' on the hosting ArcGIS Online web,

– through the CHMI mobile application.

The operation of the FFI application was in detail assessed for the period 2017–2020, from which following conclusions may be drawn:

– routine operation of the system runs without problems, though the calculations are time consuming and require adequate hardware,

– input data must be subject to regular operational quality checks (which applies particularly to rain gauge data), which would reduce some significant errors in the system outputs,

– adjusted radar QPEs were mostly overestimated, which caused, under some circumstances, incorrect assessment of the flash flood risk (false alarms),

– satellite data could be used to guess the initial conditions as well as to regularly verify the state of soil saturation,

– the operation of the FFI will further be thoroughly assessed in order to better specify its parameters and to optimize the calculation procedures.

As part of the research project "Hydrometeorological risks in the Czech Republic – changes and prediction enhancements" implemented since 2019, a new method of adjusting radar data has been developed. This method, based on spatially variable adjusting coefficient, will significantly refine precipitation estimates and reduce the number of false alarms based on already acquired experience.

The next expected improvement of precipitation estimates is related to the data from the MERGE method, when 1-hour MERGE sums are interpolated into shorter intervals.

Radar precipitation estimates based on the new adjustment method as well as the interpolated 1-hour MERGE in a time step of 10 minutes have already been prepared and entered into the FFI calculations since the convective season 2022. Due to the radical qualitative change in the input data, a detailed evaluation of this season will be carried out before the start of the convective season 2023.

The authors plan to update this document depending on the future development of the Flash Flood Indicator.

8. References

BOROVIČKA, P. et al., 2020. Project VH20172020017 Prevention of safety risks from extreme weather phenomena – their specification and innovation of prediction and warning systems with regard to climate change (Summary research report summarizing results of project solution). Prague: Czech Hydrometeorological Institute.

DAŇHELKA, J., JANÁL, P., ŠERCL, P., 2015. Possibilities of Prediction of Flash Floods in the Conditions of the Czech Republic, In: *Transaction of the CHMI*. Prague: Czech Hydrometeorological Institute. ISBN 978-80-87577-27-1.

DINGMAN, S. L., 2002. Physical Hydrology. 2nd ed., Prentice Hall, Upper Saddle River, NJ, ISBN 978-0-13-099695-4.

GOUDENHOOFDT, E., DELOBBE, L., 2009. Evaluation of Radar-Gauge Merging Methods for Quantitative Precipitation Estimates. In: *Hydrol. Earth Syst. Sci.*, Vol. **13**, p. 195–203, doi:10.5194/hess-13-195-2009.

HAWKINS, R. H., 1978. Runoff Curve Numbers with Varying Site Moisture. J. Irrig. Drain. Div. 1978, Vol. **104**, p. 389–398, doi:10.1061/JRCEA4.0001221.

KOHUT, M., HORA, P., CHUCHMA, F., 2011. Potential evapotranspiration of grass surface in location Pánov, Hodonín region – long-term trend in period 1961–2099. In: *Microclimate and Mesoclimate of Landscape Structures and Anthropogenic Environments*. Prague: Czech Hydrometeorological Institute. ISBN 978-80-86690-87-2.

KOVÁŘ, P., 1990. Utilization of Hydrological Models for Determination of Maximum Flow Rates in Small Catchments. Prague: Czech University of Agriculture. ISBN 978-80-213-0088-0.

NOAA, 2010. Flash Flood Early Warning System Reference Guide. The University Corporation for Atmospheric Research, Silver Spring, MD. ISBN 978-0-615-37421-5.

NOVÁK, P., 2007. The Czech Hydrometeorological Institute's Severe Storm Nowcasting System. In: *Atmospheric Res.*, Vol. 83, p. 450–457, doi:10.1016/j.atmosres.2005.09.014.

NOVÁK, P., 2016. CZRAD – the Modern Dual Polarization Czech Weather Radar Network. In: *Proceedings of the Geospatial, Hydrometeorological and GNSS (GEOMETOC) Workshop*, 19 – 21 October 2016. Progress Partners Advertising, Prague.

NOVÁK, P., BŘEZKOVÁ, L., FROLÍK, P., 2009. Quantitative Precipitation Forecast Using Radar Echo Extrapolation. In: *Atmospheric Research*, Vol. 93, p. 328–334, doi:10.1016/j.atmosres.2008.10.014.

NOVÁK, P., KRÁČMAR, J., 2001. Vertical Reflectivity Profiles in the Czech Weather Radar Network. In: *Preprint of Proceedings of 30th International Conference on Radar Meteorology* [CD-ROM], American Meteorological Society, Boston, MA, USA, p. P15.3.

NOVÁK, P., KYZNAROVÁ, H., 2014. Progress in Operational Quantitative Precipitation Estimation in the Czech Republic. In: *Proceedings of the ERAD 2014 – The 8th European Conference on Radar in Meteorology and Hydrology*, Garmisch-Partenkirchen, Germany, 1 – 5 September 2014, DLR Institute of Atmospheric Physics, Garmisch-Partenkirchen, Germany.

NOVÁK, P., KYZNAROVÁ, H., 2016. MERGE2 - the upgraded system of quantitative precipitation estimates operated at the Czech Hydrometeorological Institute. In: *Meteorological Bulletin*, Vol. **69**, p. 137–144, ISSN 0026-1173, https://www.chmi.cz/files/portal/docs/reditel/SIS/casmz/assets/2016/chmu_mz_5-16.pdf.

NOVÁK, P., KYZNAROVÁ, H., 2016. Upgrade of the CZRAD meteorological radar network in 2015. In: *Meteorological Bulletin*, Vol. **69**, p. 17–24, https://www.chmi.cz/files/portal/docs/reditel/SIS/casmz/assets/2016/chmu_mz_1-16.pdf.

NOVÁK, P., KYZNAROVÁ, H., PECHA, M., ŠERCL, P., SVOBODA, V., LEDVINKA, O., 2021. Utilization of Weather Radar Data for the Flash Flood Indicator Application in the Czech Republic. In: Remote Sens., Vol. 13, p. 3184, doi:10.3390/rs13163184.

OMONDI, S., 2017. What Is Torrential Rain? In: *WorldAtlas*. Reunion Technology, St. Laurent, Quebec, Canada. Also Available from WWW: https://www.worldatlas.com/articles/what-is-torrential-rain.html.

ŘEZÁČOVÁ, D., NOVÁK, P., KAŠPAR, M., SETVÁK, M., 2007. Physics of Clouds and Precipitation. Prague: Academia. ISBN 978-80-200-1505-1.

ŘIČICOVÁ, P. et al., 2007. Project VaV 1D/1/5/05 "Development of methods of prediction of drought conditions and flood situations based on infiltration and retention properties of soil cover of the Czech Republic". Prague: Czech Hydrometeorological Institute.

ŠÁLEK, M., BŘEZKOVÁ, L., NOVÁK, P., 2006. The Use of Radar in Hydrological Modeling in the Czech Republic – Case Studies of Flash Floods. In: *Nat. Hazards Earth Syst. Sci.*, Vol. **6**, p. 229–236, doi:10.5194/nhess-6-229-2006.

ŠERCL, P. et al., 2011. Development of a robust method for estimating runoff from heavy rainfall. Project SP/1c4/16/07 “Research and implementation of new tools for flood and runoff forecasting in the framework of flood warning and forecasting services in the Czech Republic”. Prague: Czech Hydrometeorological Institute.

ŠERCL, P., 2009. Influence of Physical-Geographical Factors on the Characteristics of Theoretical Design Flood Waves. In: *Transaction of the CHMI.* Prague: Czech Hydrometeorological Institute. ISBN 978-80-86690-62-9.

SOUKALOVÁ, E., 2002. Causal rainfall and floods in the Blansko and Žďár regions in July 2002. In: *Meteorological Bulletin*, Vol. **55**, p. 141–145. Prague: Czech Hydrometeorological Institute. ISSN 0026-1173. Also Available from WWW: https://www.chmi.cz/files/portal/docs/reditel/SIS/casmz/assets/2002/Meteo-2002-05.pdf

STRAUB, T. D., MELCHING, C. S., KOCHER, K. E., 2000. Equations for Estimating Clark Unit-Hydrograph Parameters for Small Rural Watersheds in Illinois. Water-Resources Investigations Report, US Geological Survey, Urbana, IL. Also Available from WWW: https://pubs.er.usgs.gov/publication/wri004184.

SWEENEY, T. L., 1992. Modernized Areal Flash Flood Guidance. NOAA Technical Memorandum NWS HYDRO; National Weather Service Office of Hydrology: Silver Spring, MD. Also Available from WWW: https://www.weather.gov/media/owp/oh/hdsc/docs/TM44.pdf.

USACE, 1994. Flood-Runoff Analysis. Engineer Manual; Department of the Army: Washington, DC. Also Available from WWW: https://www.publications.usace.army.mil/portals/76/publications/engineermanuals/em_1110-2-1417.pdf.

FLASH FLOOD INDICATOR

Petr Sercl, Martin Pecha, Petr Novak, Hana Kyznarova,
Ondrej Ledvinka, Vojtech Svoboda, Jan Danhelka

Czech Hydrometeorological Institute, Na Sabatce 2050/17, 143 06 Prague 12

Prague 2023, 52 pages

ISBN 978-80-7653-050-8